Electromagnetic field of a charge moving in a cold magnetized plasma

Sergey N. Galyamin,* Dmitry Ya. Kapshtan, and Andrey V. Tyukhtin†
Physics Department, St. Petersburg State University, St. Petersburg, 198504, Russia
(Received 12 October 2012; published 30 January 2013)

The present paper addresses the electromagnetic field generated by a point charge or a small charged particle bunch moving with constant velocity in a cold magnetized plasma, along the external magnetic field. Attention is focused on the case of ultrarelativistic motion. The field surrounding the point charge is investigated both analytically and numerically. In the analytical study, we obtain rigorous decomposition of the field into quasistatic and wave components. Beating behavior in the far-field zone and harmonic behavior in the vicinity of the charge trajectory are found using suitable approximate approaches. The transverse component of the electric field exhibits a strong (inversely proportional) singularity on the charge trajectory, while the longitudinal components of both the electric and magnetic fields exhibit a weaker (logarithmic) singularity. An efficient numerical approach is developed to calculate the field for arbitrary parameters. An efficient algorithm for calculating the fields of small bunches with different forms is also presented, using a thin charged disk and a charged cylinder as representative examples.

DOI: 10.1103/PhysRevE.87.013109 PACS number(s): 52.35.Hr, 41.60.Bq, 41.75.Lx

I. INTRODUCTION

S. I. Vavilov and P. A. Cherenkov pioneered the study of the radiation processes from the movement of charged particles in materials in the 1930s [1]. Subsequent research has resulted in the mastery of Vavilov-Cherenkov radiation (VCR) and its application in many areas of physics [2–7]. Another important radiation phenomenon, transition radiation, has also been predicted, analyzed, and put into practice [8,9]. Over the past few years, increasing attention has been given to radiation from charged particles moving in metamaterials. Metamaterials are artificial periodic structures considered to be "effective" media [10–18]. A series of interesting effects has been noted in these cases, such as reversed VCR in a left-handed medium [10–12] and reversed Cherenkov-transition radiation excited by a charge flying into the medium [13,14]. Intriguing effects are also known to occur in a so-called "wire metamaterial," where VCR can be "nondivergent" [17,18].

The radiation of moving charges in complex "traditional" media can also produce unusual phenomena, but these problems have not been analyzed sufficiently in the scientific literature up to now. In this paper, a cold magnetized plasma is considered to be an anisotropic gyrotropic medium [19] (from the point of view of macroscopic electrodynamics). The radiation processes in such a medium play an important role in accelerator physics, radioscience, cosmic ray physics, and other areas. Studies on VCR in such a medium were initiated in the 1950s [20–23] and have not yet abated [24,25]. Results have been presented in reviews and monographs [4–6], but attention has mainly focused on analyzing the particular energetic characteristics of radiation, without considering the structure of the field. There are related papers [15,16] on uniaxial anisotropic media and less closely related papers [2,26–29] on isotropic media, including left-handed media. The main goal of this paper is to study the structure of the field surrounding a charge moving in a gyrotropic anisotropic medium, which has not been analyzed previously.

The paper is organized as follows. Section II presents known integral expressions for the field components of the charge moving in an arbitrary anisotropic gyrotropic medium, along the main axis of the medium. General properties of these expressions and various equivalent forms are discussed. Section III is devoted to charge movement in a cold magnetized plasma, along the external magnetic field. The specific frequency dispersion is utilized, and the field is decomposed into quasistatic and wave components. The wave component is analyzed using two approximations in the far-field zone and in the vicinity of the charge trajectory. In Sec. IV, an exact numerical approach is presented along with the most successful numerical results for both point charge and two types of bunches. Appendices A and B contain mathematical details of the two approximations discussed in Sec. III.

II. ANALYTICAL RESULTS

A. General expressions for the field components

We consider the electromagnetic field of a point charge q moving with constant velocity υ in a medium described by the dielectric permittivity tensor

$$\hat{\varepsilon} = \begin{pmatrix} \varepsilon_1 & -i\varepsilon_2 & 0 \\ i\varepsilon_2 & \varepsilon_1 & 0 \\ 0 & 0 & \varepsilon_3 \end{pmatrix} \tag{1}$$

and magnetic permeability $\mu = 1$. Here, ε_1, ε_2, and ε_3 are assumed to be frequency dependent, i.e., frequency dispersion is taken into account. The ε_2 component causes gyrotropy, while the inequality of components ε_1 and ε_3 creates uniaxial anisotropy. We assume that the charge moves along the optical axis, which coincides with the z axis of the cylindrical frame of reference, ρ, φ, z. Thus, the charge and current densities have the form

$$\rho^{\mathrm{q}} = q\delta(\rho)\delta(z - \upsilon t), \quad \vec{j} = \upsilon\rho^{\mathrm{q}}\vec{e}_z. \tag{2}$$

*galiaminsn@yandex.ru
†tyukhtin@bk.ru

Expressions for the electromagnetic field components, based on Maxwell's equations, can be easily obtained using the Fourier transform [21]. Omitting tedious calculations, we write these expressions in the following form:

$$\begin{Bmatrix} E_\rho \\ E_\varphi \\ E_z \end{Bmatrix} = \int_{-\infty}^{+\infty} \begin{Bmatrix} e_\rho(\omega) \\ e_\varphi(\omega) \\ e_z(\omega) \end{Bmatrix} \exp\left(i\omega\frac{\zeta}{\upsilon}\right) d\omega,$$
$$\begin{Bmatrix} H_\rho \\ H_\varphi \\ H_z \end{Bmatrix} = \int_{-\infty}^{+\infty} \begin{Bmatrix} h_\rho(\omega) \\ h_\varphi(\omega) \\ h_z(\omega) \end{Bmatrix} \exp\left(i\omega\frac{\zeta}{\upsilon}\right) d\omega, \tag{3}$$

where

$$\begin{Bmatrix} e_\rho(\omega) \\ e_\varphi(\omega) \\ e_z(\omega) \end{Bmatrix} = \begin{Bmatrix} e_\rho^{(e)}(\omega) - e_\rho^{(o)}(\omega) \\ e_\varphi^{(e)}(\omega) - e_\varphi^{(o)}(\omega) \\ e_z^{(e)}(\omega) - e_z^{(o)}(\omega) \end{Bmatrix},$$
$$\begin{Bmatrix} h_\rho(\omega) \\ h_\varphi(\omega) \\ h_z(\omega) \end{Bmatrix} = \begin{Bmatrix} h_\rho^{(e)}(\omega) - h_\rho^{(o)}(\omega) \\ h_\varphi^{(e)}(\omega) - h_\varphi^{(o)}(\omega) \\ h_z^{(e)}(\omega) - h_z^{(o)}(\omega) \end{Bmatrix}, \tag{4}$$

$$e_\rho^{(o,e)} = \frac{-iq}{2\beta c^3}\frac{\omega^2 s_{o,e} H_1^{(1)}(\rho s_{o,e})}{\varepsilon_1\left(s_e^2 - s_o^2\right)}\left(\varepsilon_1 - \frac{1}{\beta^2} - \frac{c^2 s_{o,e}^2}{\omega^2}\right), \tag{5}$$

$$e_\varphi^{(o,e)} = -\frac{q}{2\beta c^3}\omega^2\varepsilon_2\frac{s_{o,e} H_1^{(1)}(\rho s_{o,e})}{\varepsilon_1\left(s_e^2 - s_o^2\right)}, \tag{6}$$

$$e_z^{(o,e)} = \frac{q}{2c^2}\frac{\omega}{\varepsilon_1\left(s_e^2 - s_o^2\right)} H_0^{(1)}(\rho s_{o,e})\left[\frac{\omega^2}{c^2}\left(\varepsilon_1^2 - \varepsilon_2^2 - \frac{2\varepsilon_1}{\beta^2} + \frac{1}{\beta^4}\right) + s_{o,e}^2\left(\frac{1}{\beta^2} - \varepsilon_1\right)\right], \tag{7}$$

$$h_\rho^{(o,e)} = \frac{q}{2\beta^2 c^3}\omega^2\varepsilon_2\frac{s_{o,e} H_1^{(1)}(\rho s_{o,e})}{\varepsilon_1\left(s_e^2 - s_o^2\right)}, \tag{8}$$

$$h_\varphi^{(o,e)} = \frac{iq}{2c^3}\frac{\omega^2 s_{o,e} H_1^{(1)}(\rho s_{o,e})}{\varepsilon_1\left(s_e^2 - s_o^2\right)} \times \left(\varepsilon_2^2 - \varepsilon_1^2 + \frac{c^2\varepsilon_1 s_{o,e}^2}{\omega^2} + \frac{\varepsilon_1}{\beta^2}\right), \tag{9}$$

$$h_z^{(o,e)} = \frac{iq}{2\beta c^2}\omega\varepsilon_2\frac{s_{o,e}^2 H_0^{(1)}(\rho s_{o,e})}{\varepsilon_1\left(s_e^2 - s_o^2\right)}. \tag{10}$$

Here, c is the velocity of light, $\beta = \upsilon/c$, $\zeta = z - \upsilon t$, and $H_{0,1}^{(1)}(\xi)$ is the Hankel function. The squared orthogonal wave vectors $s_{o,e}^2$ are solutions of the dispersion equation

$$k_\rho^4\frac{\omega^2}{c^2}\varepsilon_1 - k_\rho^2\left[\left(\frac{\omega^2}{c^2}\varepsilon_1 - k_z^2\right)(\varepsilon_1 + \varepsilon_3)\frac{\omega^2}{c^2} - \varepsilon_2^2\frac{\omega^4}{c^4}\right] - \frac{\omega^2\varepsilon_3}{c^2}\left[\varepsilon_2^2\frac{\omega^4}{c^4} - \left(k_z^2 - \frac{\varepsilon_1\omega^2}{c^2}\right)^2\right] = 0 \tag{11}$$

with respect to k_ρ^2, given that the longitudinal wave vector component is $k_z = \omega/\upsilon$:

$$s_{o,e}^2 = \frac{-B \pm \sqrt{B^2 - 4\varepsilon_1 C}}{2\varepsilon_1}, \tag{12}$$

$$B = \frac{\omega^2}{c^2}\left[\varepsilon_2^2 - \left(\varepsilon_1 - \frac{1}{\beta^2}\right)(\varepsilon_1 + \varepsilon_3)\right], \tag{13}$$

$$C = \frac{\omega^4\varepsilon_3}{c^4}\left[\left(\varepsilon_1 - \frac{1}{\beta^2}\right)^2 - \varepsilon_2^2\right], \tag{14}$$

where the lower sign corresponds to the index "o" and the upper sign corresponds to the index "e." The elements $\varepsilon_{1,2,3}$ are complex when there are losses in the medium so the orthogonal components $s_{o,e}$ of the wave vector must be determined (at real frequencies) by the rule

$$s_{o,e}(\omega) = \sqrt{s_{o,e}^2(\omega)}, \quad \operatorname{Im} s_{o,e}(\omega) > 0. \tag{15}$$

This rule guarantees the exponential decay of the waves in (3) with increasing ρ. A medium with negligible losses can be considered as a limiting case.

Equation (11) can also be written in more common equivalent form with respect to the refractive index $n = c\omega^{-1}k$ (see, for example, Ref. [21])

$$\frac{\omega^2}{c^2}(\varepsilon_1\sin^2\theta + \varepsilon_3\cos^2\theta) \times \left[n^2 - n_o^2(\theta)\right]\left[n^2 - n_e^2(\theta)\right] = 0, \tag{16}$$

where θ is the angle between the main crystal axis (z axis) and the wave vector $\vec{k}$, and $n_{o,e}$ are the refractive indexes of the ordinary and extraordinary waves, respectively,

$$n_{o,e}^2 = \left[\left(\varepsilon_1^2 - \varepsilon_2^2\right)\sin^2\theta + \varepsilon_1\varepsilon_3(1 + \cos^2\theta) \pm \sqrt{\sin^4\theta\left(\varepsilon_1^2 - \varepsilon_2^2 - \varepsilon_1\varepsilon_3\right)^2 + 4\varepsilon_2^2\varepsilon_3^2\cos^2\theta}\right] \times \left[2(\varepsilon_1\sin^2\theta + \varepsilon_3\cos^2\theta)\right]^{-1}, \tag{17}$$

where the upper sign corresponds to the index "o" and the lower sign corresponds to the index "e." Using (12), one can find the angles $\theta_{o,e}$ between $\vec{k}_{o,e} = \vec{e}_\rho s_{o,e} + \vec{e}_z\omega/\upsilon$ and the z axis:

$$\tan\theta_{o,e} = \upsilon s_{o,e}/\omega. \tag{18}$$

Expressions (12) may be transformed as follows:

$$s_{o,e}^2 = \omega^2\left[n_{o,e}^2(\theta_{o,e})\beta^2 - 1\right]/\upsilon^2, \tag{19}$$

i.e., the function s_o corresponds to an ordinary wave and the function s_e corresponds to an extraordinary wave. Therefore, the summands with indexes "o" and "e" in formulas (4)–(10) correspond to ordinary and extraordinary waves. Note that each expression in (19) formally coincides with an expression for the orthogonal component of the wave vector in an isotropic medium [14,15,29].

B. Alternative expressions for the field components

General properties of the integrands can be obtained from (12)–(15). The integrals in (3) may be simplified by restricting the integration interval to only positive frequencies. It is well

known that if Fourier transform $f(\omega)$ of the real function $F(t)$ is given by

$$f(\omega)=\frac{1}{2\pi}\int_{-\infty}^{+\infty}F(t)\exp(i\omega t)\,dt,$$

then $f(-\bar{\omega})=\overline{f(\omega)}$, where the overbar indicates the complex conjugate. Because all field components are necessarily real, one obtains

$$e_{\rho,\varphi,z}(-\bar{\omega})=\overline{e_{\rho,\varphi,z}(\omega)}, \tag{20}$$

$$h_{\rho,\varphi,z}(-\bar{\omega})=\overline{h_{\rho,\varphi,z}(\omega)}. \tag{21}$$

Based on (20) and (21), it can be shown that

$$\int_{\Gamma}f(\omega)\exp\left(i\omega\frac{\zeta}{\upsilon}\right)d\omega=2\mathrm{Re}\int_{\Gamma_+}f(\omega)\exp\left(i\omega\frac{\zeta}{\upsilon}\right)d\omega, \tag{22}$$

where Γ is an arbitrary contour that is symmetrical with respect to the imaginary axis, Γ_+ is the part of Γ in the half-plane $\mathrm{Re}\omega>0$, and $f(\omega)$ can correspond to any of the functions in (4). When Γ is the real axis, the integrals in (3) reduce to

$$\begin{Bmatrix}E_{\rho,\varphi,z}\\H_{\rho,\varphi,z}\end{Bmatrix}=2\mathrm{Re}\int_{0}^{+\infty}\begin{Bmatrix}e_{\rho,\varphi,z}(\omega)\\h_{\rho,\varphi,z}(\omega)\end{Bmatrix}\exp\left(i\omega\frac{\zeta}{\upsilon}\right)d\omega. \tag{23}$$

The integrands in (23) contain both ordinary and extraordinary waves, in which case only positive frequencies are relevant for calculating the field. When there are no losses, the parts of the real positive semiaxis where $\mathrm{Im}\,s_o=0$ or $\mathrm{Im}\,s_e=0$ correspond to propagating waves of one type or another.

Further simplifications are achieved by using the relationship between functions s_o and s_e. We assume that medium (1) has some losses. Because $\varepsilon_1(-\bar{\omega})=\overline{\varepsilon_1(\omega)}$, $i\varepsilon_2(-\bar{\omega})=\overline{i\varepsilon_2(\omega)}$, and $\varepsilon_3(-\bar{\omega})=\overline{\varepsilon_3(\omega)}$ [30], we have, for functions (13) and (14),

$$B(-\bar{\omega})=\overline{B(\omega)},\quad C(-\bar{\omega})=\overline{C(\omega)}. \tag{24}$$

Note that the inner radical in (12) can be defined arbitrarily because (12) produces all solutions of (11) independently by this definition. Let us define this radical by the rule $\mathrm{Im}\sqrt{B^2(\omega)-4\varepsilon_1(\omega)C(\omega)}>0$ in the entire complex ω plane, resulting in the following property:

$$\sqrt{B^2(-\bar{\omega})-4\varepsilon_1(-\bar{\omega})C(-\bar{\omega})}=-\overline{\sqrt{B^2(\omega)-4\varepsilon_1(\omega)C(\omega)}}. \tag{25}$$

Based on (24) and (25), the following property can be easily proven:

$$s_o^2(-\bar{\omega})=\overline{s_e^2(\omega)},$$

hence,

$$s_o(-\bar{\omega})=\pm\overline{s_e(\omega)}. \tag{26}$$

Because (15) must be fulfilled for both $s_o(-\bar{\omega})$ and $s_e(\omega)$, one should choose the minus sign in (26) to yield

$$s_o(-\bar{\omega})=-\overline{s_e(\omega)}\quad\text{or}\quad s_e(-\bar{\omega})=-\overline{s_o(\omega)}. \tag{27}$$

Property (27) facilitates obtaining an alternative representation for the field components, which include only one of the functions $s_{o,e}$. Using (27) and the properties of the Hankel function $H_0^{(1)}(-\bar{z})=-\overline{H_0^{(1)}(z)}$, $H_1^{(1)}(-\bar{z})=\overline{H_1^{(1)}(z)}$ [31], one obtains

$$e^{(o)}_{\rho,\varphi,z}(-\bar{\omega})=\overline{e^{(e)}_{\rho,\varphi,z}(\omega)},\quad h^{(o)}_{\rho,\varphi,z}(-\bar{\omega})=\overline{h^{(e)}_{\rho,\varphi,z}(\omega)}. \tag{28}$$

Using (28), for an arbitrary contour Γ, which is symmetrical with respect to the imaginary axis, we obtain

$$\int_{\Gamma}f(\omega)\exp(i\omega\zeta/\upsilon)\,d\omega=\mp2\mathrm{Re}\int_{\Gamma}f^{(o,e)}(\omega)\exp(i\omega\zeta/\upsilon)\,d\omega, \tag{29}$$

where $f(\omega)$ corresponds to any of the functions in (4) and $f^{(o,e)}(\omega)$ are the summands of $f(\omega)$. For the particular case of integration over the real axis, one obtains the following equivalent forms of the integrals (3):

$$\begin{Bmatrix}E_{\rho,\varphi,z}\\H_{\rho,\varphi,z}\end{Bmatrix}=\mp2\mathrm{Re}\int_{-\infty}^{+\infty}\begin{Bmatrix}e^{(o,e)}_{\rho,\varphi,z}(\omega)\\h^{(o,e)}_{\rho,\varphi,z}(\omega)\end{Bmatrix}\exp\left(i\omega\frac{\zeta}{\upsilon}\right)d\omega, \tag{30}$$

where the upper sign corresponds to the index "o" while the lower sign corresponds to the index "e." Representation (30) contains only one of the functions $s_{o,e}$, but unlike (23), integration is performed over the entire real axis. Note that the positive and negative semiaxes play different roles in (30): Positive frequencies correspond to waves of one type, while negative frequencies correspond to waves of another type. For example, if we choose the upper-sign term from (30) (with only "extraordinary" integrands), then positive frequencies correspond to extraordinary waves, while negative frequencies correspond to ordinary waves.

Let us investigate the behavior of integrands in (30) for $|\omega|\to\infty$. Because $\varepsilon_1(\omega)$ and $\varepsilon_3(\omega)$ tend to unity while $\varepsilon_2(\omega)$ tends to zero [30], one obtains from (12)–(15) that

$$\begin{aligned}&s_{o,e}^2\xrightarrow[|\omega|\to\infty]{}-\frac{\omega^2(1-\beta^2)}{\beta^2c^2},\\&s_{o,e}\xrightarrow[|\omega|\to\infty]{}i\frac{\sqrt{1-\beta^2}}{\beta c}\omega\mathrm{sgn}(\mathrm{Re}\omega).\end{aligned} \tag{31}$$

Using asymptotic expressions for the Hankel functions $H_{0,1}^{(1)}(\xi)$ as $|\xi|\to\infty$ [31], one can extract the exponential term from the integrands in (30):

$$\begin{Bmatrix}e^{(o,e)}_{\rho,\varphi,z}(\omega)\\h^{(o,e)}_{\rho,\varphi,z}(\omega)\end{Bmatrix}\exp\left(i\omega\frac{\zeta}{\upsilon}\right)\underset{|\omega|\to\infty}{\sim}\exp\left[-\frac{\rho\sqrt{1-\beta^2}}{\beta c}\omega\mathrm{sgn}(\mathrm{Re}\omega)+i\omega\frac{\zeta}{\beta c}\right]. \tag{32}$$

As follows from (32), the integrands in (30) vanish at $|\omega|\to\infty$ in the following sectors of the complex ω plane:

$$\begin{aligned}&\mathrm{Im}\,\omega>-|\mathrm{Re}\omega|\frac{\rho\sqrt{1-\beta^2}}{\zeta}\quad\text{for}\quad\zeta>0,\\&\mathrm{Im}\,\omega<|\mathrm{Re}\omega|\frac{\rho\sqrt{1-\beta^2}}{|\zeta|}\quad\text{for}\quad\zeta<0.\end{aligned} \tag{33}$$

Moreover, the asymptotes of the steepest descent path (SDP) can be easily found using (32). These asymptotes lie in the

sectors given by (33) and are determined by the expression

$$\mathrm{Im}\,\omega = |\mathrm{Re}\omega|\zeta/(\rho\sqrt{1-\beta^2}), \tag{34}$$

which is similar to the results for an isotropic medium [14,15,29] and an anisotropic nongyrotropic medium [16].

III. THE CASE OF A COLD MAGNETIZED PLASMA

A. General expressions

A model for a cold electron plasma in an external magnetic field is utilized here. The frequency dependence of the components of the permittivity tensor in such a medium is described by the following expressions [19]:

$$\begin{aligned}\varepsilon_1(\omega) &= 1 - \frac{\omega_p^2(\omega+i\nu)}{\omega\left[(\omega+i\nu)^2-\omega_h^2\right]},\\ \varepsilon_2(\omega) &= \frac{-\omega_p^2\omega_h}{\omega\left[(\omega+i\nu)^2-\omega_h^2\right]},\\ \varepsilon_3(\omega) &= 1 - \frac{\omega_p^2}{\omega^2+i\omega\nu},\end{aligned} \tag{35}$$

where $\omega_p^2 = 4\pi Ne^2/m$ is the plasma frequency (N is the electron density and e and m are the electron charge and the electron mass, respectively), $\omega_h = |e|H_{\mathrm{ext}}/(mc)$ is a "gyrofrequency" (H_{ext} is the external magnetic field), and ν is the effective collision frequency. The following analytical calculations are performed for the case where the medium has no losses ($\nu = 0$) but an infinitely small value of ν can be used, if needed, to determine the branches of the radicals and the positional relationship of the integration path and the singularities. Using (12) and (35), the functions $s_{o,e}^2(\omega)$ can be presented in the form

$$\begin{aligned}s_{o,e}^2 = \Bigg[(1-\beta^2)\left(-\omega^4+\omega^2\omega_\Sigma^2-\frac{\omega_p^2\omega_h^2}{2}\right)+\beta^2\omega_p^4-\beta^2\omega^2\omega_p^2\\ \mp\beta\omega_p^2\omega_h\sqrt{\omega^2-\omega_c^2}\Bigg](\beta c)^{-2}\left(\omega^2-\omega_\Sigma^2\right)^{-1},\end{aligned} \tag{36}$$

where the upper sign corresponds to the index "o" and the lower sign corresponds to the index "e" and

$$\omega_\Sigma = \sqrt{\omega_p^2+\omega_h^2}, \quad \omega_c^2 = \omega_p^2 - \omega_h^2\frac{(1-\beta^2)^2}{4\beta^2}. \tag{37}$$

As seen from (37),

$$\mathrm{sgn}\omega_c^2 = \mathrm{sgn}(\beta-\beta_0), \quad \beta_0 \equiv \frac{\sqrt{\omega_p^2+\omega_h^2}-\omega_p}{\omega_h}. \tag{38}$$

The branch point $\omega_c = \sqrt{\omega_c^2}$ may thus be determined as follows:

$$\omega_c > 0 \ \text{ for } \ \beta > \beta_0, \quad \mathrm{Im}\,\omega_c > 0 \ \text{ for } \ \beta < \beta_0. \tag{39}$$

B. Properties of the $s_\pm(\omega)$ functions in the complex plane

The integrals in (30) can be calculated using complex function theory. For this the behavior of these integrands should be investigated over the complex ω plane. The first step is to determine the radical $\sqrt{\omega^2-\omega_c^2}$ to fulfill the requirement

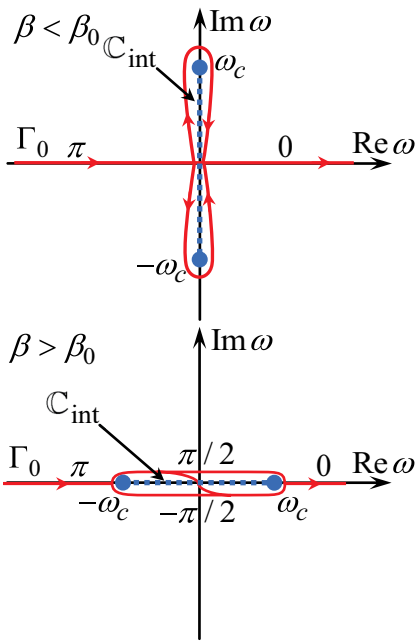

FIG. 1. (Color online) The cut $\mathbb{C}_{\mathrm{int}}$ of the radical $\sqrt{\omega^2-\omega_c^2}$ in the complex ω plane and the initial integration path Γ_0 for $\beta < \beta_0$ (top) and $\beta > \beta_0$ (bottom). The digits indicate the argument of the radical.

given by (25). The branch points $\pm\omega_c$, connected by the cut $\mathbb{C}_{\mathrm{int}}$, allows determining the radical by the requirement

$$\sqrt{\omega^2-\omega_c^2} \to \omega \quad \text{for} \quad |\omega| \to \infty. \tag{40}$$

For $\beta > \beta_0$, the branch points $\pm\omega_c$ are real and $\mathbb{C}_{\mathrm{int}}$ lies on the real axis, while for $\beta < \beta_0$, the branch points $\pm\omega_c$ are imaginary and $\mathbb{C}_{\mathrm{int}}$ lies on the imaginary axis (see Fig. 1). It is easy to prove that the initial integration path Γ_0 can bypass both the upper and the lower banks of $\mathbb{C}_{\mathrm{int}}$. Indeed, let us start from the initial representation (3) and consider integral over the closed contour around $\mathbb{C}_{\mathrm{int}}$ (in the case $\beta > \beta_0$ for definiteness):

$$\begin{aligned}\Delta F = &\int_{\substack{-\omega_c\\ \text{top bank}}}^{\omega_c} f(\omega)\exp\left(i\omega\frac{\zeta}{\upsilon}\right)d\omega\\ &+\int_{\substack{\omega_c\\ \text{bottom bank}}}^{-\omega_c} f(\omega)\exp\left(i\omega\frac{\zeta}{\upsilon}\right)d\omega,\end{aligned} \tag{41}$$

where $f(\omega)$ corresponds to any of the functions in (4). For $\beta > \beta_0$, the values of the radical $\sqrt{\omega^2-\omega_c^2}$ at the top bank (t.b.) and at the bottom bank (b.b.) are connected by the formulas

$$\begin{aligned}\sqrt{\omega^2-\omega_c^2}|_{\mathrm{b.b.}} &= -\sqrt{\omega^2-\omega_c^2}|_{\mathrm{t.b.}},\\ s_{o,e}(\omega)|_{\mathrm{b.b.}} &= s_{e,o}(\omega)|_{\mathrm{t.b.}},\\ f^{(o)}(\omega)|_{\mathrm{b.b.}} &= -f^{(e)}(\omega)|_{\mathrm{t.b.}},\\ f(\omega)|_{\mathrm{b.b.}} &= f(\omega)|_{\mathrm{t.b.}},\end{aligned} \tag{42}$$

and, therefore, $\Delta F = 0$, proving the statement. Moreover, as was just demonstrated, the integrands in (3) have no singularity on $\mathbb{C}_{\mathrm{int}}$ and the integration path Γ_0 can "jump" from the upper bank to the lower one at any arbitrary point within $\mathbb{C}_{\mathrm{int}}$. Similar relationships can be found for $\beta < \beta_0$, for the left bank (l.b.)

and for the right bank (r.b.):

$$\begin{aligned} s_{o,e}(\omega)|_{\text{l.b.}} &= s_{e,o}(\omega)|_{\text{r.b.}}, \\ f^{(o)}(\omega)|_{\text{l.b.}} &= -f^{(e)}(\omega)|_{\text{r.b.}}, \\ f(\omega)|_{\text{l.b.}} &= f(\omega)|_{\text{r.b.}}. \end{aligned} \tag{43}$$

Thus, the integration path Γ_0 can bypass $\mathbb{C}_{\text{int}}$ both from below and above or "jump" from the left bank to the right one at any arbitrary point within the cut. Because (29) is valid for an arbitrary Γ, which is symmetrical with respect to the imaginary axis, representation (30) is also valid for the integration path Γ_0 passing $\mathbb{C}_{\text{int}}$ from above or from below.

Formula (36) shows that the two other candidates for singularities in the functions $s_{o,e}(\omega)$ are the branch points $\omega = \pm\omega_\Sigma$, where the denominator of (36) tends to zero. The next step is to determine the roots of the numerator in (36):

$$\begin{aligned} &(1-\beta^2)\left(-\omega^4 + \omega^2\omega_\Sigma^2 - \omega_p^2\omega_h^2/2\right) + \beta^2\omega_p^4 \\ &\quad - \beta^2\omega^2\omega_p^2 \mp \beta\omega_p^2\omega_h\sqrt{\omega^2-\omega_c^2} = 0. \end{aligned} \tag{44}$$

Expression (44) is a transcendental equation that cannot be solved directly, so we will use a trick to solve it. Let us start with the successive approximation method for $\omega_h \ll \omega_p$, $\omega_h \ll \omega$ as a small parameter. In the zeroth-order approximation ($\omega_h = 0$), equation (44) can be written as

$$\omega^4(\beta^2-1) - \omega^2\left(2\beta^2\omega_p^2\right) + \beta^2\omega_p^4 = 0 \tag{45}$$

with roots

$$[\omega^{(0)}]^2 = \omega_p^2, \quad [\omega^{(0)}]^2 = -\frac{\beta^2\omega_p^2}{1-\beta^2}. \tag{46}$$

Let us find the first-order correction to $[\omega^{(0)}]^2 = \omega_p^2$ using the following ansatz:

$$[\omega^{(1)}]^2 = \omega_p^2 + \alpha\omega_h^2.$$

Substituting this expression into (44) and taking into account terms $\sim\omega_h^2$, one obtains an equation for α

$$-2\omega_p^2\alpha \pm 2\beta\omega_p^2\sqrt{\alpha + \frac{(1-\beta^2)^2}{4\beta^2}} + \omega_p^2(1-\beta^2) = 0,$$

with the following solutions:

$$\alpha_1 = 0, \quad \alpha_2 = 1.$$

Thus, in the first-order approximation, the roots of (44) are $[\omega_1^{(1)}]^2 = \omega_p^2$ and $[\omega_2^{(1)}]^2 = \omega_\Sigma^2$. By using the ansatz $[\omega^{(2)}]^2 = \omega_p^2 + \alpha\omega_h^2 + \eta\omega_h^4$, one finds that the correction of order $\eta\omega_h^4$ equals zero. This result hints that the roots found thus far are the exact roots. Indeed, direct substitution shows that $\omega = \omega_p$ and $\omega = -\omega_\Sigma$ are exact roots of (44) with the plus sign, while $\omega = -\omega_p$ and $\omega = \omega_\Sigma$ are exact roots of (44) with the minus sign.

Because two roots of (44) have just been found exactly, the other roots can also be found. For this purpose, let us substitute variables in (44):

$$\sqrt{\omega^2-\omega_c^2} \equiv u \quad \Rightarrow \quad \omega^2 = u^2 + \omega_c^2. \tag{47}$$

Recall that from the definition of $\sqrt{\omega^2-\omega_c^2}$ (40), the signs of u and ω are equal in the region of reality for u. The left-hand side of (44) is a fourth-degree polynomial in u, with two known roots. The residual two roots can be found as usual to obtain

$$\begin{aligned} s_o^2 &= -\frac{(1-\beta^2)(u+u_1)(u+u_3)(u+u_4)}{\beta^2c^2(u+u_2)}, \\ s_e^2 &= -\frac{(1-\beta^2)(u-u_1)(u-u_3)(u-u_4)}{\beta^2c^2(u-u_2)}, \end{aligned} \tag{48}$$

where

$$u_{1,2} = \frac{\omega_h(1\mp\beta^2)}{2\beta}, \tag{49}$$

$$u_{3,4} = \frac{\omega_h\beta}{2} \mp \frac{1}{\beta}\sqrt{\frac{\omega_h^2}{4} - \frac{\omega_p^2\beta^2}{1-\beta^2}}. \tag{50}$$

The numerators in (48) have only three roots, while the denominators have only one root, due to cancellation of identical multipliers in the numerator and the denominator of the original expression. Note that $u = u_j$ for $\omega = \omega_j$ ($j = 1,2,3,4$), where

$$\omega_1 = \omega_p, \quad \omega_2 = \omega_\Sigma, \tag{51}$$

$$\omega_{3,4} = \frac{\omega_h}{2} \mp \sqrt{\frac{\omega_h^2}{4} - \frac{\omega_p^2\beta^2}{1-\beta^2}}. \tag{52}$$

It should be stressed that although we started with the method of successive approximations, we have obtained the exact roots of (44) in the end, which can be easily proven by direct substitution.

The radical in (50) and (52) is real at

$$\beta \leqslant \beta_1 \equiv \frac{\omega_h}{\sqrt{\omega_h^2 + 4\omega_p^2}}, \tag{53}$$

and it is imaginary for $\beta > \beta_1$ (it can be easily shown that $\beta_1 > \beta_0$ at arbitrary values of ω_p and ω_h). Let us define this radical in the following way:

$$\begin{aligned} &\text{Im}\sqrt{\frac{\omega_h^2}{4} - \frac{\omega_p^2\beta^2}{1-\beta^2}} > 0 \quad \text{for} \quad \beta > \beta_1, \\ &\text{Re}\sqrt{\frac{\omega_h^2}{4} - \frac{\omega_p^2\beta^2}{1-\beta^2}} \geqslant 0 \quad \text{for} \quad \beta \leqslant \beta_1. \end{aligned} \tag{54}$$

For $\beta > \beta_1$, the branch points ω_3 and ω_4 are complex, with ω_4 lying in the upper half-plane, ω_3 lying in the lower half-plane, and $\text{Re}\omega_{3,4} = \omega_h/2$. For $\beta = \beta_1$, $\omega_3 = \omega_4 = \omega_h/2$. For $\beta < \beta_1$, the branch points ω_3 and ω_4 are real with $0 < \omega_3 < \omega_h/2$ and $\omega_4 > \omega_h/2$. From (48), the function $s_e^2(\omega)$ always has two zeros, $\omega = \omega_1 = \omega_p$ and $\omega = \omega_4$, and one pole at $\omega = \omega_2 = \omega_\Sigma$. The function $s_o^2(\omega)$ always has two zeros, $\omega = -\omega_1 = -\omega_p$ and $\omega = -\omega_4$, and one pole at $\omega = -\omega_2 = -\omega_\Sigma$. The third zero is more complicated because it depends on the charge velocity. For $\beta > \beta_1$, the function $s_e^2(\omega)$ has a zero at $\omega = \omega_3$, while the function $s_o^2(\omega)$ has a zero at $\omega = -\omega_3$. For $\beta < \beta_1$, a certain velocity β' ($\beta_0 < \beta' < \beta_1$) exists such that $u_3 = 0$ for $\beta = \beta'$, $u_3 < 0$ for $\beta < \beta'$, and $u_3 > 0$ for $\beta' < \beta < \beta_1$ (a cumbersome expression for β' derived using symbolic computer calculation is not given here). Therefore, in addition to the aforementioned poles and zeros, the function s_e^2 has a zero at $\omega = -\omega_3$ for $\beta < \beta'$ and a zero at $\omega = \omega_3$ for

$\beta' < \beta < \beta_1$. Similarly, the function s_o^2 has a zero at $\omega = \omega_3$ for $\beta < \beta'$ and a zero at $\omega = -\omega_3$ for $\beta' < \beta < \beta_1$. For $\beta = \beta'$, the branch point ω_3 coincides with ω_c. The zeros and poles of the function $s_e^2(\omega)$ are situated symmetrically with respect to those of the function $s_o^2(\omega)$ with respect to the imaginary axis. For $\beta \to 0$, one obtains $\omega_3 \to 0$ and $\omega_4 \to \omega_h$.

C. The case of ultrarelativistic velocities

We now consider the case where the charge velocity β is so high that the inequality $\beta > \beta_1$ is fulfilled at arbitrary values of ω_p and ω_h. For definiteness, we will refer to this case as the case of ultrarelativistic velocities [we can be sure that the inequality $\beta > \beta_1$ is fulfilled at $\gamma \equiv (1-\beta^2)^{-1/2} \gg 1$]. Because the functions $s_{o,e}(\omega)$ are determined by the rule given in (15), cuts may be taken in segments where $\operatorname{Im} s_{o,e} = 0$. Figure 2 shows the positional relationship of the original integration path, the branch points, and the cuts of function $s_e(\omega)$ [the cuts and singularities of $s_o(\omega)$ can be obtained by reflecting those of $s_e(\omega)$ with respect to the imaginary axis].

It has been shown above that the cut $\mathbb{C}_{\text{int}}$ has no effect on the calculation of the field. This fact is illustrated in Fig. 2, where the initial contour Γ_0 can pass the cut $\mathbb{C}_{\text{int}}$ from above or below. It is more significant that the function $s_e(\omega)$ has a cut on the real

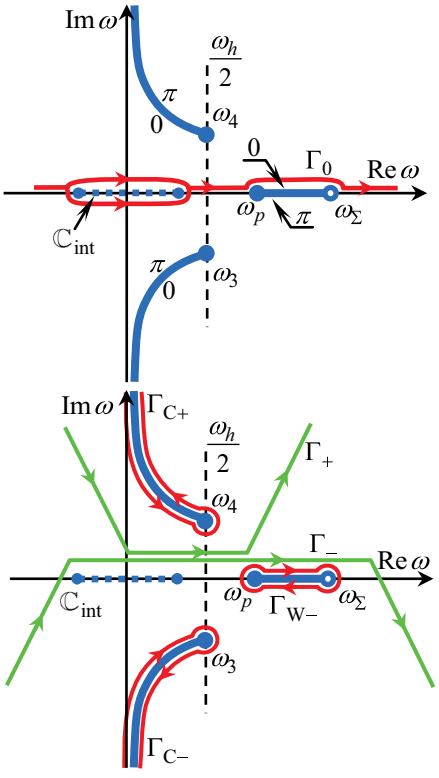

FIG. 2. (Color online) Branch points (ω_p, ω_Σ, ω_3, and ω_4) and cuts of the function $s_e(\omega)$ on the complex ω plane for $\beta > \beta_1$. The contour Γ_0 is the original integration path, which is transformed to Γ_{C+} (for analytical manipulation) or Γ_+ (for numerical calculation) in the domain $\zeta > 0$ (in front of the charge) and to $\Gamma_{C-} + \Gamma_{W-}$ (for analytical manipulations) or Γ_- (for numerical calculations) in the domain $\zeta < 0$ (behind the charge). The numbers 0 and π indicate the argument of s_e on the corresponding cut banks.

axis between the branch points ω_p and ω_Σ, where $\operatorname{Im} s_e(\omega) = 0$. By being situated on the positive semiaxis, the cut corresponds to the radiated extraordinary waves. It can be shown by a limiting process from the case with losses that the initial contour Γ_0 should pass the upper bank of this cut where $s_e > 0$.

From (33), the integration path in (30) can be complemented by a semicircle of an infinite radius in the upper half-plane for $\zeta > 0$ (in front of the charge) and in the lower half-plane for $\zeta < 0$ (behind the charge). Following this manipulation, the field can be expressed as an integral over the contours encircling the cuts: Γ_{C+} in front of charge and $\Gamma_{C-} + \Gamma_{W-}$ behind the charge (Fig. 2). These integrals can be rewritten as integrals over the single cut bank. After a series of transformations, we obtain

$$\begin{Bmatrix} E_{\rho,\varphi,z} \\ H_{\rho,\varphi,z} \end{Bmatrix} = \begin{Bmatrix} E^C_{\rho,\varphi,z} + E^W_{\rho,\varphi,z} \\ H^C_{\rho,\varphi,z} + H^W_{\rho,\varphi,z} \end{Bmatrix}, \tag{55}$$

$$\begin{Bmatrix} E^W_\rho \\ E^W_\varphi \\ E^W_z \end{Bmatrix} = \Phi(-\zeta) \int_{\omega_p}^{\omega_\Sigma} \begin{Bmatrix} \tilde{e}_\rho J_1(\rho s_e) \sin\left(\frac{\omega\zeta}{\upsilon}\right) \\ \tilde{e}_\varphi J_1(\rho s_e) \cos\left(\frac{\omega\zeta}{\upsilon}\right) \\ \tilde{e}_z J_0(\rho s_e) \cos\left(\frac{\omega\zeta}{\upsilon}\right) \end{Bmatrix} d\omega, \tag{56}$$

$$\begin{Bmatrix} H^W_\rho \\ H^W_\varphi \\ H^W_z \end{Bmatrix} = \Phi(-\zeta) \int_{\omega_p}^{\omega_\Sigma} \begin{Bmatrix} \tilde{h}_\rho J_0(\rho s_e) \cos\left(\frac{\omega\zeta}{\upsilon}\right) \\ \tilde{h}_\varphi J_1(\rho s_e) \sin\left(\frac{\omega\zeta}{\upsilon}\right) \\ \tilde{h}_z J_0(\rho s_e) \sin\left(\frac{\omega\zeta}{\upsilon}\right) \end{Bmatrix} d\omega, \tag{57}$$

$$\begin{Bmatrix} E^C_\rho \\ E^C_\varphi \\ E^C_z \end{Bmatrix} = \int_{\omega_4}^{+i\infty} \begin{Bmatrix} \operatorname{Im}\left[\tilde{e}_\rho J_1(\rho s_e) \exp\left(\frac{i\omega|\zeta|}{\upsilon}\right) d\omega\right] \\ \operatorname{Re}\left[\tilde{e}_\varphi J_1(\rho s_e) \exp\left(\frac{i\omega|\zeta|}{\upsilon}\right) d\omega\right] \operatorname{sgn}\zeta \\ \operatorname{Re}\left[\tilde{e}_z J_0(\rho s_e) \exp\left(\frac{i\omega|\zeta|}{\upsilon}\right) d\omega\right] \operatorname{sgn}\zeta \end{Bmatrix}, \tag{58}$$

$$\begin{Bmatrix} H^C_\rho \\ H^C_\varphi \\ H^C_z \end{Bmatrix} = \int_{\omega_4}^{+i\infty} \begin{Bmatrix} \operatorname{Re}\left[\tilde{h}_\rho J_1(\rho s_e) \exp\left(\frac{i\omega|\zeta|}{\upsilon}\right) d\omega\right] \operatorname{sgn}\zeta \\ \operatorname{Im}\left[\tilde{h}_\varphi J_1(\rho s_e) \exp\left(\frac{i\omega|\zeta|}{\upsilon}\right) d\omega\right] \\ \operatorname{Im}\left[\tilde{h}_z J_0(\rho s_e) \exp\left(\frac{i\omega|\zeta|}{\upsilon}\right) d\omega\right] \end{Bmatrix}, \tag{59}$$

where

$$\tilde{e}_\rho = \frac{qc}{\omega_p^2 \omega_h} \frac{s_e(\omega^2 - \omega_h^2)}{\sqrt{\omega^2 - \omega_c^2}} \left(s_e^2 + \frac{\omega^2}{\upsilon^2} - \frac{\omega^2}{c^2}\varepsilon_1 \right), \tag{60}$$

$$\tilde{e}_z = \frac{q\beta}{\omega_p^2 \omega_h} \frac{\omega(\omega^2 - \omega_h^2)}{\sqrt{\omega^2 - \omega_c^2}} \left[s_e^2 \left(\varepsilon_1 - \frac{1}{\beta^2} \right) + \frac{\omega^2}{c^2} \left(\varepsilon_2^2 - \varepsilon_1^2 + \frac{2\varepsilon_1}{\beta^2} - \frac{1}{\beta^4} \right) \right], \tag{61}$$

$$\tilde{e}_\varphi = -\beta \tilde{h}_\rho = -q\omega s_e / \left(c\sqrt{\omega^2 - \omega_c^2} \right), \tag{62}$$

$$\tilde{h}_\varphi = \frac{qc\beta}{\omega_p^2 \omega_h} \frac{s_e(\omega^2 - \omega_h^2)}{\sqrt{\omega^2 - \omega_c^2}} \left[\varepsilon_1 s_e^2 + \frac{\omega^2}{c^2} \left(\varepsilon_2^2 - \varepsilon_1^2 + \frac{\varepsilon_1}{\beta^2} \right) \right], \tag{63}$$

$$\tilde{h}_z = -q s_e^2 / \sqrt{\omega^2 - \omega_c^2}, \tag{64}$$

and $\Phi(-\zeta)$ is the Heaviside step function. The integration is performed over the upper cut bank (where $s_e > 0$) in (56) and

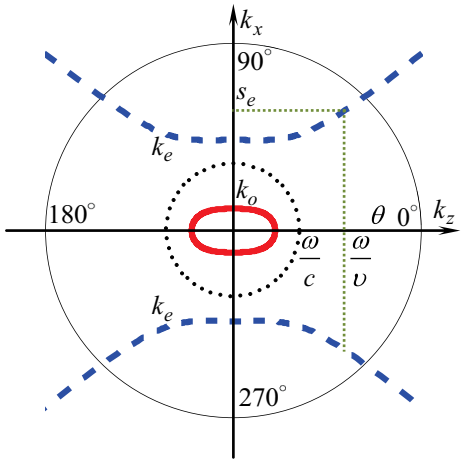

FIG. 3. (Color online) Wave vectors for the ordinary k_o and extraordinary k_e waves at $\omega_h/\omega_p = 0.5$ ($\omega_\Sigma = 1.12\omega_p$) and $\omega = 1.06\omega_p$.

(57) and over the right-hand cut bank (where $s_e < 0$) in (58) and (59).

As mentioned above, only the extraordinary wave is generated by the moving charge in the case under consideration. This fact can be further illustrated if we use the following expressions for the refractive indexes $n_{o,e}(\theta)$ in a cold magnetized plasma [19]:

$$n_{o,e}^2 = 1 - 2\omega_p^2\left(\omega^2 - \omega_p^2\right)\left[2\left(\omega^2 - \omega_p^2\right)\omega^2 - \omega_h^2\omega^2\sin^2\theta \pm \sqrt{\omega^4\omega_h^4\sin^4\theta + 4\omega_h^2\omega^2\left(\omega^2 - \omega_p^2\right)^2\cos^2\theta}\right]^{-1}.$$

Figure 3 shows the polar plot of $k_o(\theta) = \omega n_o(\theta)/c$ and $k_e(\theta) = \omega n_e(\theta)/c$ versus θ at a certain frequency between ω_p and ω_Σ. These curves can be interpreted at the same time as the dependencies $k_{xo,e}(k_z)$. For the field of moving charge, $k_z = \omega/\upsilon > \omega/c$. Figure 3 shows that the curve $k_o(\theta)$ lies entirely inside the circle $k = \omega/c$ so there is no real solution for s_o. In contrast, the curve $k_e(\theta)$ lies entirely outside the circle $k = \omega/c$ so a real solution for s_e exists at arbitrary velocity β. The physical meaning of these conclusions is the following: because $k_o < \omega/c$, the phase velocity of the ordinary wave, is larger than c, $\upsilon_{pho} = \omega/k_o > c$. Therefore, this is a fast wave that cannot be excited by a charge moving slower than light. In contrast, the phase velocity of the extraordinary wave is less than c, $\upsilon_{phe} = \omega/k_e < c$, indicating that the wave is slow and is excited by the moving charge.

Based on (58), (59), and (60)–(64), one can analytically estimate the region of significance of the quasistatic field. Because the integration path is along the cut in the upper half-plane, the term $\exp(i\omega|\zeta|/\upsilon)$ describes the exponential decay of the integrands with increasing $|\zeta|$. It is obvious that the main contribution to the integral comes from the vicinity of point ω_4 so the nonexponential term can be factored out of the integral. The residual integral involving the exponent can be calculated along the ray starting at ω_4 and reaching $\mathrm{Re}\omega_4 + i\infty$, parallel to the imaginary axis. The quasistatic field components acquire the exponential term $\exp(-\mathrm{Im}\,\omega_4|\zeta|/\upsilon)$, which determines the region of significance of the quasistatic field:

$$|\zeta| < \zeta_C \equiv \beta c/\mathrm{Im}\,\omega_4 \underset{\gamma\gg 1}{\approx} c/(\omega_p\gamma). \tag{65}$$

As will be shown below, the estimation by (65) is in good agreement with the numerical results for the ultrarelativistic case for values of $\gamma \sim 10$ and larger. It should be noted that the contour in the form of the ray from ω_4 up to $\mathrm{Re}\omega_4 + i\infty$ can be utilized in numerical calculations of the quasistatic field.

Despite the fact that the decomposition given by (55) is easy to understand, the numerical calculation of the wave components by the formulas (56), (57), and (60)–(64) is rather difficult for at least a number of components. As shown in Sec. III D and Appendix A, the singular behavior of the function $s_e(\omega)$ at $\omega \to \omega_\Sigma$ leads to poor convergence of the integrals for the wave components. We overcome this difficulty in two ways. The first method consists of obtaining approximate analytical expressions for the wave components in the vicinity of the charge motion line (Sec. III D) or in the far-field zone (Sec. III E). The second method consists of developing a numerical approach suitable for calculating the entire field for arbitrary parameters (Sec. IV).

D. Wave field in the vicinity of the charge motion line

Let us now investigate the behavior of the wave components in (56) and (57) for small values of ρ. Henceforth, the approach described in this section will be referred to as the "small ρ approach." The main difficulty with computing the integrals in (56) and (57) is that the function $s_e(\omega)$, as given by (48), tends to infinity as $\omega \to \omega_\Sigma$:

$$s_e^2(\omega) \underset{\omega\to\omega_\Sigma - 0}{\approx} \sigma_e^2/(\omega_\Sigma - \omega), \tag{66}$$

where

$$\sigma_e^2 = \omega_p^2\omega_h^2(1+\beta^2)/(2\beta^2c^2\omega_\Sigma). \tag{67}$$

This behavior leads to the divergence of some of the field components at $\rho \to 0$. The detailed treatment of this divergence is given in Appendix A. The following approximate expressions have been obtained:

$$E_\rho^W \underset{\rho\to 0}{\approx} E_\rho^{W1}\left(\frac{\rho\omega_p}{c}\right)^{-1},$$

$$\begin{Bmatrix} E_z^W \\ H_z^W \end{Bmatrix} \underset{\rho\to 0}{\approx} \begin{Bmatrix} E_z^{W0} \\ H_z^{W0} \end{Bmatrix} + \begin{Bmatrix} E_z^{W1} \\ H_z^{W1} \end{Bmatrix} \ln\left(\frac{\rho\omega_p}{c}\right), \tag{68}$$

$$\begin{Bmatrix} E_\varphi^W \\ H_{\rho,\varphi}^W \end{Bmatrix} \underset{\rho\to 0}{\approx} \frac{\rho\omega_p}{c}\left[\begin{Bmatrix} E_\varphi^{W0} \\ H_{\rho,\varphi}^{W0} \end{Bmatrix} + \begin{Bmatrix} E_\varphi^{W1} \\ H_{\rho,\varphi}^{W1} \end{Bmatrix} \ln\left(\frac{\rho\omega_p}{c}\right)\right], \tag{69}$$

where the dominant contributions take the form

$$E_\rho^{W1} = \frac{2q\omega_p^3}{c^2\beta\omega_\Sigma}\sin\left(\frac{\omega_\Sigma\zeta}{\upsilon}\right), \tag{70}$$

$$E_z^{W1} = \frac{2q\omega_p^2}{c^2\beta^2}\cos\left(\frac{\omega_\Sigma\zeta}{\upsilon}\right), \tag{71}$$

$$H_z^{W1} = \frac{2q\omega_p^2\omega_h}{c^2\beta\omega_\Sigma}\sin\left(\frac{\omega_\Sigma\zeta}{\upsilon}\right), \tag{72}$$

$$E_\varphi^{W1} = \frac{q\omega_p\omega_h}{c^2\beta}\cos\left(\frac{\omega_\Sigma\zeta}{\upsilon}\right) = -\beta H_\rho^{W1}, \tag{73}$$

$$H_\varphi^{W1} = \frac{q\omega_p\omega_h^2}{c^2\beta^2\omega_\Sigma}\sin\left(\frac{\omega_\Sigma\zeta}{\upsilon}\right), \tag{74}$$

while the corrections to the dominant contributions can be found in Appendix A.

As seen from (68) and (69), the E_ρ^W component possesses a strong singularity ($\sim\rho^{-1}$), while the E_z^W and H_z^W components each possess a weak logarithmic singularity. The other components vanish $\sim\rho\ln\rho$ as $\rho\to 0$. Moreover, (70)–(74) show that all the components behave harmonically with frequency ω_Σ in the vicinity of the charge motion line.

It is worthwhile to compare the field behavior in the neighborhood of the charge motion line given by (68) and (69) with that for the cold plasma in the absence of an external magnetic field, the dielectric permittivity of which is given by

$$\varepsilon(\omega) = 1 - \omega_p^2/\omega^2. \tag{75}$$

The electric field for this case is known to consist of a quasistatic field and a so-called "plasma trace" (plasma oscillations) [4,29]. The "plasma trace" is described by the following expressions:

$$\begin{aligned} E_\rho^P &= \frac{2q\omega_p^2}{\upsilon^2} K_1\left(\rho\frac{\omega_p}{\upsilon}\right)\sin\left(\frac{\omega_p\zeta}{\upsilon}\right),\\ E_z^P &= -\frac{2q\omega_p^2}{\upsilon^2} K_0\left(\rho\frac{\omega_p}{\upsilon}\right)\cos\left(\frac{\omega_p\zeta}{\upsilon}\right), \end{aligned} \tag{76}$$

where $K_{0,1}$ are the modified Bessel functions (McDonald functions). Using the asymptotic behavior of the functions $K_{0,1}$ at $\rho\to 0$ [31], one obtains

$$\begin{aligned} E_\rho^P &\underset{\rho\to 0}{\approx} \frac{2q\omega_p^2}{c^2\beta}\sin\left(\frac{\omega_p\zeta}{\upsilon}\right)\left(\frac{\rho\omega_p}{c}\right)^{-1},\\ E_z^P &\underset{\rho\to 0}{\approx} \frac{2q\omega_p^2}{c^2\beta^2}\cos\left(\frac{\omega_p\zeta}{\upsilon}\right)\ln\left(\frac{\rho\omega_p}{c}\right). \end{aligned} \tag{77}$$

Expressions (68) for $E_{\rho,z}^W$ are reduced to (77) as $\omega_h\to 0$, which is quite natural.

As one can see from (77), the field of "plasma trace" contains only transversal and longitudinal electric components possessing singularities at $\rho\to 0$ ($\sim\rho^{-1}$ or $\sim\ln\rho$). Thus, the singular behavior of the wave field components (68) is analogous to the singular behavior of the "plasma trace" (77) (despite of difference in derivations, because (76) results from computation of residues in poles $\omega=\pm\omega_p$ [29], while (68) is determined by contribution of small vicinity of $\omega=\omega_\Sigma$ to the integrals for wave components). The essential physical distinction of the wave field produced by point charge moving in magnetized plasma is that it contains magnetic components $H_{\rho,z}^W$, with the longitudinal component H_z^W possessing a logarithmic singularity.

To further illustrate the influence of the external magnetic field on the field of the moving charge in the vicinity of the charge trajectory, we now consider the ω_h dependence of the magnitude of the harmonic functions E_ρ^{W1} (70), E_z^{W1} (71), and H_z^{W1} (72) (note that the correction terms E_ρ^{W0}, E_z^{W0}, and H_z^{W0} can be neglected for small-enough ρ). First, the magnitude of the longitudinal electric field E_z^{W1} equals $2q\omega_p^2/\upsilon^2$ and is independent of ω_h (and correspondingly B_{ext}), i.e., the magnitude of this component in the magnetized plasma coincides with that in the plasma without a magnetic field. However, the magnitude of the orthogonal electric field

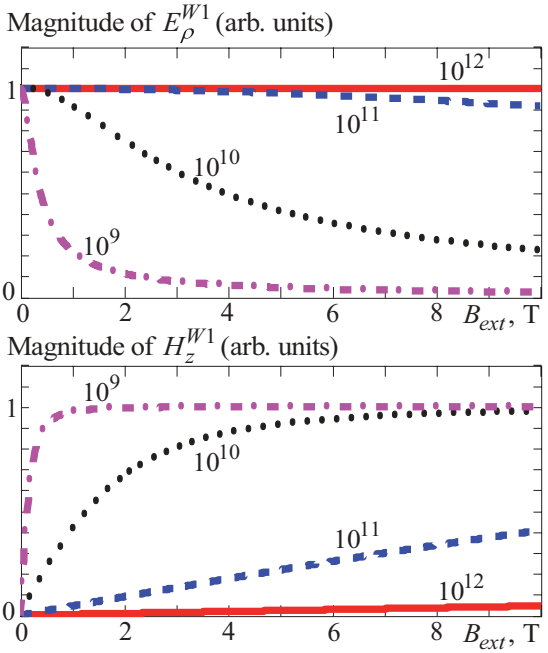

FIG. 4. (Color online) The magnitude $2q\omega_p^3/(c^2\beta\omega_\Sigma)$ of the orthogonal electric field (top) and the magnitude of the longitudinal magnetic field $2q\omega_p^2\omega_h/(c^2\beta\omega_\Sigma)$ (bottom) behind the charge near the charge trajectory versus B_{ext}. Various plasma frequency values $\omega_p/(2\pi)$ (s^{-1}) are indicated near the curves.

E_ρ^{W1} equals $2q\omega_p^3/(c^2\beta\omega_\Sigma)$ and can be reduced essentially by the external magnetic field (Fig. 4). As mentioned above, B_{ext} produces H_z^{W1} with a magnitude $2q\omega_p^2\omega_h/(c^2\beta\omega_\Sigma)$ that increases significantly with an increase in B_{ext} (Fig. 4).

Using the main terms in (68) and (69), one obtains the components of the Poynting vector $\vec{S}=c/(4\pi)[\vec{E},\vec{H}]$:

$$S_\rho^W \underset{\rho\to 0}{\approx} \frac{c}{4\pi}\left(E_\varphi^{W1}H_z^{W1} - E_z^{W1}H_\varphi^{W1}\right)\frac{\rho\omega_p}{c}\left[\ln\left(\frac{\rho\omega_p}{c}\right)\right]^2, \tag{78}$$

$$\begin{aligned} S_\varphi^W &\underset{\rho\to 0}{\approx} -\frac{c}{4\pi}E_\rho^{W1}H_z^{W1}\ln\left(\frac{\rho\omega_p}{c}\right)\left(\frac{\rho\omega_p}{c}\right)^{-1},\\ S_z^W &\underset{\rho\to 0}{\approx} \frac{c}{4\pi}E_\rho^{W1}H_\varphi^{W1}\ln\left(\frac{\rho\omega_p}{c}\right). \end{aligned} \tag{79}$$

Therefore, the orthogonal flux S_ρ^W is negligible in the vicinity of the charge motion line, whereas the longitudinal flux S_z^W is large and the azimuthal flux S_φ^W is very large.

E. Wave field in the far-field zone

Let us now investigate the behavior of the wave components (56) and (57) at $\zeta<0$ and large distances ρ from the charge motion line. As in Refs. [27,28], we solve the integrals using the stationary point method [32]. We assume that ρ is sufficiently large so $\rho|s_e|\gg 1$ at the stationary points ω_s, which will be found below. Then, the Bessel functions can be replaced by their asymptotic expressions [31], and the wave components (56) and (57) can be presented as integrals with the rapidly oscillating functions $\exp[i\rho s_e(\omega)\pm i\omega|\zeta|/\upsilon]$. The

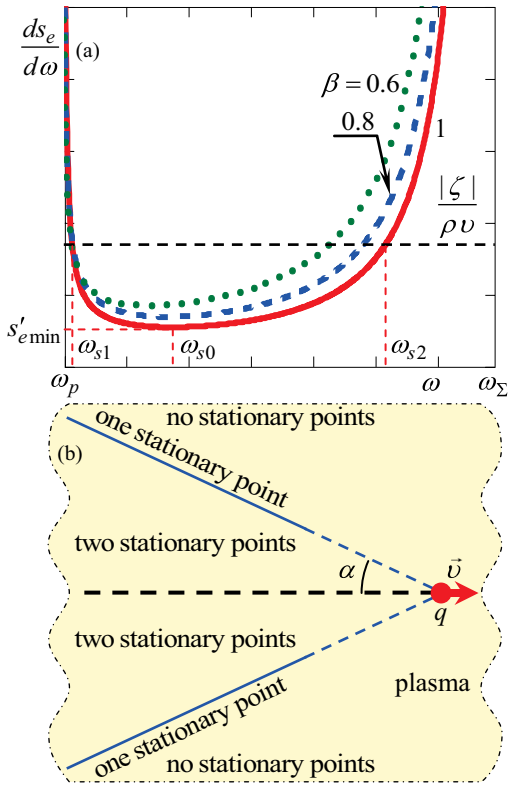

FIG. 5. (Color online) Illustration of the solution of equation (81) for the stationary points. The typical dependence of $ds_e/d\omega$ on ω, for various β values, with the calculated stationary points $\omega_{s1,2}$ (a) and the corresponding Cherenkov cone with an apex angle α determined by $\mathrm{tg}\alpha = (\upsilon s'_{e\min})^{-1}$ (b). The dependence $ds_e/d\omega$ on ω is calculated for $\omega_h = 0.5\omega_p$.

main contribution to these integrals is given by the stationary points ω_s, which are determined by the equations below

$$\rho ds_e(\omega_s)/d\omega \pm |\zeta|/\upsilon = 0. \tag{80}$$

The detailed investigation of (80) for the ultrarelativistic case is given in Appendix B. The first conclusion is that the function $s_e(\omega)$ increases monotonously in the interval $\omega_p < \omega < \omega_\Sigma$, i.e., $ds_e/d\omega > 0$, and (80) with the plus sign has no solutions. Therefore, we obtain the following equation for stationary points:

$$ds_e(\omega_s)/d\omega = |\zeta|/(\rho\upsilon). \tag{81}$$

The second conclusion is that when the external magnetic field is not very strong ($\omega_h < 6\sqrt{2}\omega_p \approx 8.5\omega_p$), the derivative $ds_e/d\omega$ has a minimum at $\omega = \omega_{s0}$, where $\omega_p < \omega_{s0} < \omega_\Sigma$. The typical dependence of $ds_e/d\omega$ on ω is shown in Fig. 5(a), where the cone (which can be called the Cherenkov cone) is determined by the following equation:

$$|\zeta| = \zeta_{\min}(\rho) \equiv \rho\upsilon s'_{e\min}, \quad s'_{e\min} \equiv ds_e(\omega_{s0})/d\omega_{s0}. \tag{82}$$

There are two stationary points $\omega_{s1,2}$ inside the cone ($|\zeta| > \zeta_{\min}$). There is a single stationary point ω_{s0} at the boundary of the cone ($|\zeta| = \zeta_{\min}$), and there are no stationary points outside the cone ($|\zeta| < \zeta_{\min}$) [see Fig. 4(b)]. For $|\zeta| \gg \zeta_{\min}$, one obtains $\omega_{s1} \to \omega_p$, $\omega_{s2} \to \omega_\Sigma$ and

$$\begin{aligned} \omega_{s1} &\approx \sqrt{\omega_p^2 + \left(\frac{\rho\omega_p^2}{2|\zeta|\sqrt{\omega_h}}\right)^{4/3}}, \\ \omega_{s2} &\approx \sqrt{\omega_p^2 + \left[\omega_h - \left(\frac{\rho\omega_p\omega_\Sigma}{2|\zeta|\sqrt{\omega_h}}\right)^{2/3}\right]^2}. \end{aligned} \tag{83}$$

The following asymptotic expressions can be written inside the Cherenkov cone:

$$\begin{Bmatrix} E_\rho^W \\ E_\varphi^W \\ E_z^W \end{Bmatrix} \approx \frac{1}{\rho} \begin{Bmatrix} \frac{-\tilde{e}_\rho^W(\omega_{s1})}{\sqrt{s_{e1}|s''_{e1}|}} \sin\left(\rho s_{e1} - \frac{\omega_{s1}|\zeta|}{\upsilon}\right) + \frac{\tilde{e}_\rho^W(\omega_{s2})}{\sqrt{s_{e2}|s''_{e2}|}} \cos\left(\rho s_{e2} - \frac{\omega_{s2}|\zeta|}{\upsilon}\right) \\ \frac{-\tilde{e}_\varphi^W(\omega_{s1})}{\sqrt{s_{e1}|s''_{e1}|}} \cos\left(\rho s_{e1} - \frac{\omega_{s1}|\zeta|}{\upsilon}\right) - \frac{\tilde{e}_\varphi^W(\omega_{s2})}{\sqrt{s_{e2}|s''_{e2}|}} \sin\left(\rho s_{e2} - \frac{\omega_{s2}|\zeta|}{\upsilon}\right) \\ \frac{-\tilde{e}_z^W(\omega_{s1})}{\sqrt{s_{e1}|s''_{e1}|}} \sin\left(\rho s_{e1} - \frac{\omega_{s1}|\zeta|}{\upsilon}\right) + \frac{\tilde{e}_z^W(\omega_{s2})}{\sqrt{s_{e2}|s''_{e2}|}} \cos\left(\rho s_{e2} - \frac{\omega_{s2}|\zeta|}{\upsilon}\right) \end{Bmatrix}, \tag{84}$$

$$\begin{Bmatrix} H_\rho^W \\ H_\varphi^W \\ H_z^W \end{Bmatrix} \approx \frac{1}{\rho} \begin{Bmatrix} \frac{-\tilde{h}_\rho^W(\omega_{s1})}{\sqrt{s_{e1}|s''_{e1}|}} \cos\left(\rho s_{e1} - \frac{\omega_{s1}|\zeta|}{\upsilon}\right) - \frac{\tilde{h}_\rho^W(\omega_{s2})}{\sqrt{s_{e2}|s''_{e2}|}} \sin\left(\rho s_{e2} - \frac{\omega_{s2}|\zeta|}{\upsilon}\right) \\ \frac{-\tilde{h}_\varphi^W(\omega_{s1})}{\sqrt{s_{e1}|s''_{e1}|}} \sin\left(\rho s_{e1} - \frac{\omega_{s1}|\zeta|}{\upsilon}\right) + \frac{\tilde{h}_\varphi^W(\omega_{s2})}{\sqrt{s_{e2}|s''_{e2}|}} \cos\left(\rho s_{e2} - \frac{\omega_{s2}|\zeta|}{\upsilon}\right) \\ \frac{\tilde{h}_z^W(\omega_{s1})}{\sqrt{s_{e1}|s''_{e1}|}} \cos\left(\rho s_{e1} - \frac{\omega_{s1}|\zeta|}{\upsilon}\right) + \frac{\tilde{h}_z^W(\omega_{s2})}{\sqrt{s_{e2}|s''_{e2}|}} \sin\left(\rho s_{e2} - \frac{\omega_{s2}|\zeta|}{\upsilon}\right) \end{Bmatrix}, \tag{85}$$

where $s_{e1,2} = s_e(\omega_{s1,2})$, $s''_e = d^2 s_e/d\omega^2$, and $s''_{e1,2} = s''_e(\omega_{s1,2})$. The formulas (84) and (85) show that at large distances from the charge motion line inside the cone (82), the field is essentially determined by two small frequency regions. Recall that these two frequency ranges are not associated with the ordinary and extraordinary waves. As shown below, the only extraordinary wave is excited in the case under consideration (see Sec. III C).

IV. NUMERICAL METHODS AND RESULTS

A. Field of a point charge

In this section, we describe the numerical method developed for the computation of the field components with arbitrary parameters and present representative numerical results. In the vicinity of the charge motion line, as well as in the far-field zone, the results of the exact calculations will be compared to the approximate solutions.

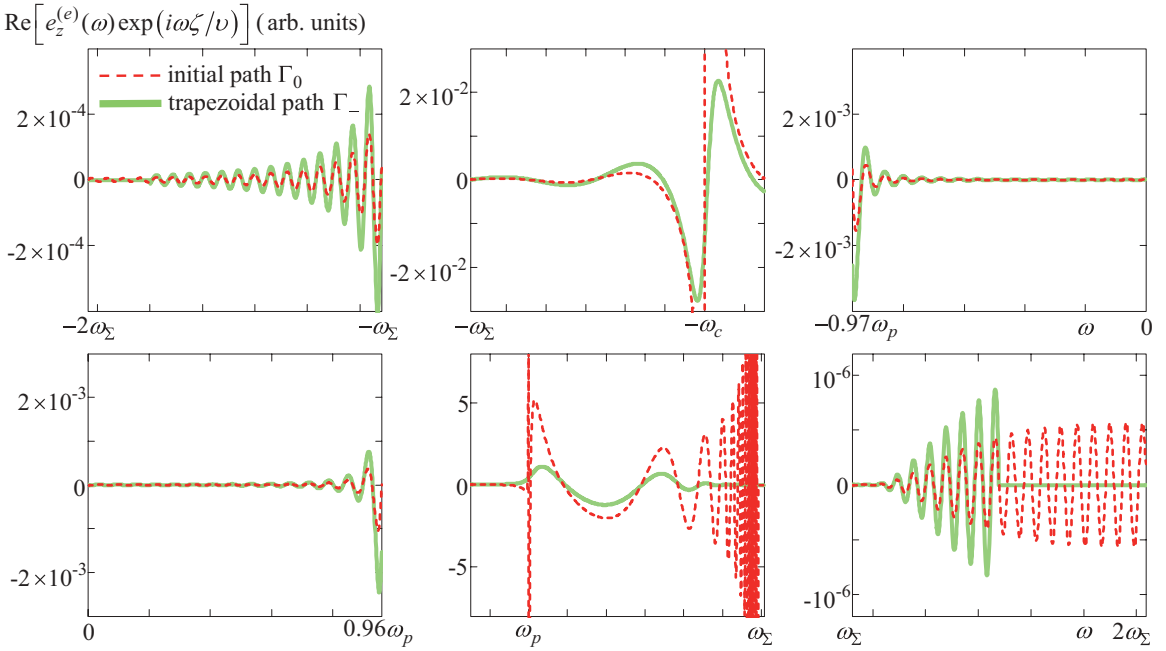

FIG. 6. (Color online) The behavior of the integrand (for the E_z component) on the original integration path Γ_0 (red dashed line) and the trapezoidal path Γ_- (green solid line), which are shown in Fig. 2. The calculation parameters are $\omega_h = 0.5\omega_p$, $\beta_1 = 0.24$, $\beta = 0.9$, $\omega_c = 0.99\omega_p$, $\rho = 20c/\omega_p$, and $\zeta = -100c/\omega_p$.

We will use the representation (30), with the s_e function, for the numerical algorithm. Knowing the singularities of the function s_e in the complex ω plane and properties (33) and (34), the original integration path Γ_0 can be suitably transformed in the complex plane to provide good convergence of the integrals (see Fig. 2). In the domain $\zeta > 0$ (in front of the moving

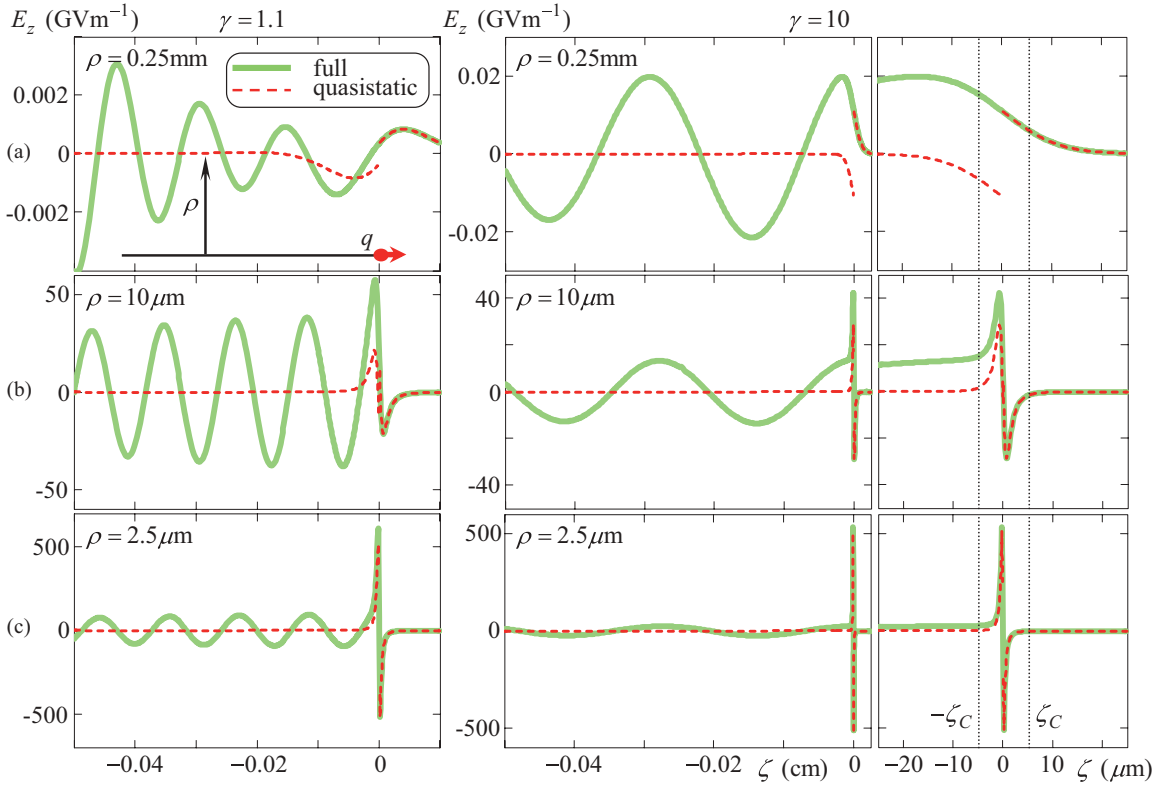

FIG. 7. (Color online) The full field (solid green line) and its quasistatic component (dashed red line) versus ζ for relatively small ζ and various ρ and γ. The calculation parameters are $q = -1$ nC, $\omega_p = 2\pi \times 10^{12}$ s^{-1}, $\omega_h = 0.5\omega_p$ ($B_{\text{ext}} \approx 18$ T), and $\nu = 10^{-4}\omega_p$.

charge), the trapezoidal path Γ_+ can be used with its semi-infinite sections parallel to the asymptotes of SDP from (34) in the upper half-plane. In the domain $\zeta < 0$ (behind the charge), the analogous trapezoidal line Γ_- bent in the lower half-plane can be utilized. Both paths should be located at a sufficient distance from the singularities in the integrands. The typical dependence of the integrands of the E_z component on the original path and on the transformed path, as parameterized by a variable along the real axis, are shown in Fig. 6. As seen from Fig. 6, the transformed path provides both a smoother behavior for the integrands and a more rapid decay of the integrands at large values of the integration variable. Smoothing can clearly be seen in the domain $[\omega_p, \omega_\Sigma]$, while the faster decay is clearly seen in the region $\omega > \omega_\Sigma$. Another benefit of this approach is

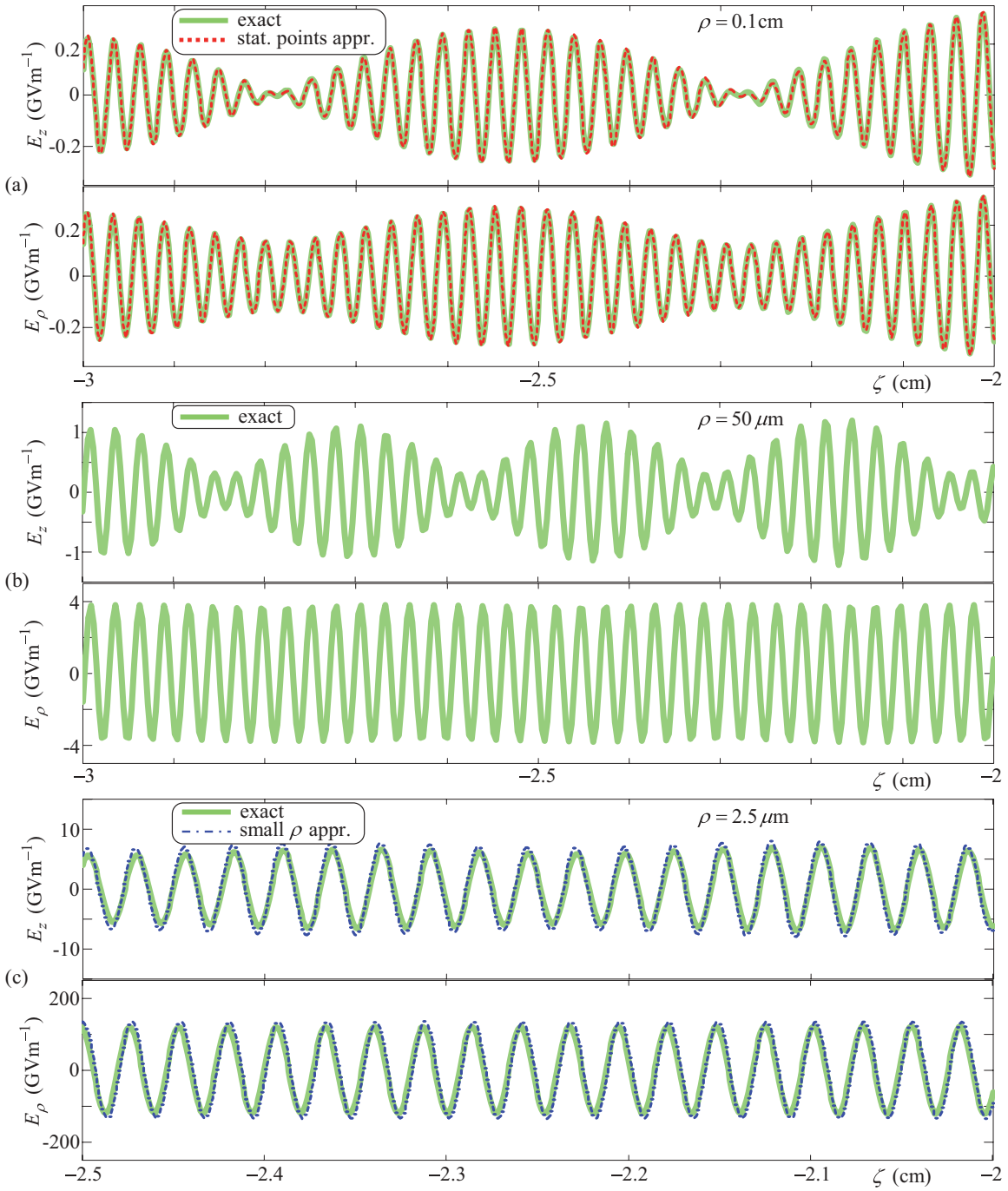

FIG. 8. (Color online) The total field from numerical calculations (solid green line), the stationary point method (dashed red line), and the small ρ approximation (dashed-dotted blue line). Plot (a) corresponds to the far-field zone, plot (b) corresponds to the middle zone, and plot (c) corresponds to the zone with small values of ρ. The calculation parameters are $q = -1$ nC, $\omega_p = 2\pi \times 10^{12}$ s^{-1}, $\omega_h = 0.5\omega_p$ ($B_{\text{ext}} \approx 18$ T), and $\gamma = 22$. For plot (a), the distances ρ and ζ have been chosen so the observation point is always inside the Cherenkov cone (82): $|\zeta| > \zeta_{\min}(\rho)$, where $\zeta_{\min} = 1.65$ cm for $\rho = 0.1$ cm. For plot (c), the distances ρ and ζ have been chosen to satisfy the requirements of the small ρ approach: $\rho < \rho_{\max}(\zeta)$, where $\rho_{\max} \in [4, 4.9]$ μm for $\zeta \in [-2.5, -2]$ cm.

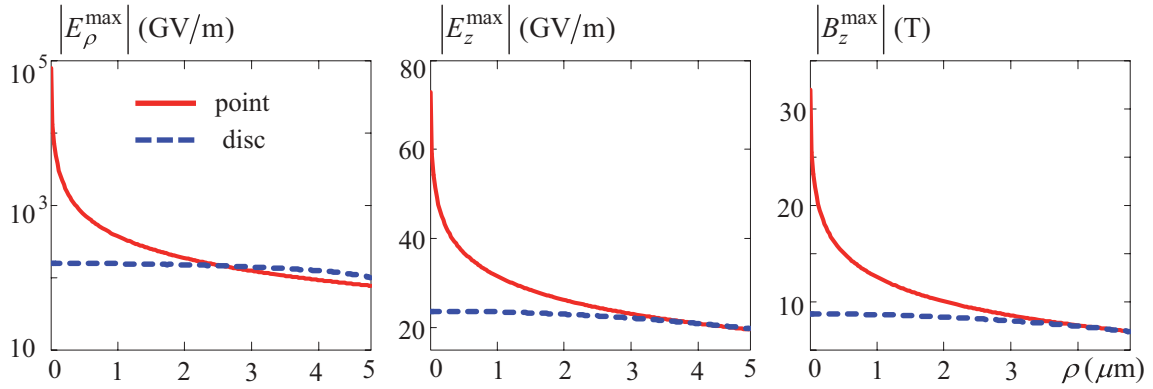

FIG. 9. (Color online) The magnitudes of the longitudinal and orthogonal electric field and the longitudinal magnetic field versus ρ, produced by a point charge (solid red line) and a charged disk with radius $a = 4.8$ μm (dashed blue line). Other calculation parameters are $q = -1$ nC, $\omega_p = 2\pi \times 10^{12}$ s^{-1}, $\omega_h = 0.14\omega_p$ ($B_{\text{ext}} = 5$ T), $\beta = 0.999$ ($\gamma = 22$), $\zeta_0 = 3.7$ cm, $\zeta = -480$ μm, and $\rho_{\max}(\zeta) = 12$ μm.

that the parameters of the transformed integration path (shift in the upper half-plane, length of the parallel to the real axis) can be adjusted to achieve the most accurate results.

Figure 7 shows the total field (in the relatively small vicinity of the charge dislocation) calculated by the numerical method described together with the quasistatic field calculated using the formulas (58) and (59). It can be seen that the total field in the region in front of the charge ($\zeta > 0$) coincides with the quasistatic field, in agreement with the predictions of the formulas (55)–(59). The quasistatic component of the longitudinal electric field has a discontinuity at $\zeta = 0$, while the total field becomes continuous. The width of the region where quasistatic field dominates is in good agreement with the theoretical estimation from (65) for large γ (the boundaries $\pm\zeta_C$ of this region are shown in the right row of Fig. 7 for the case of large γ). Figure 7(a) shows that the quasistatic field is relatively weak for large ρ. The quasistatic field becomes more significant with decreasing ρ [Fig. 7(b)] until it determines almost the total field for small ρ [Fig. 7(c)]. The larger the charge velocity β (or the Lorentz factor γ), the narrower the area over which the quasistatic field is significant.

Figure 8 shows the dependence of the longitudinal and orthogonal components of the electric field on ζ at relatively large distances behind the charge ($\zeta < 0$, $|\zeta| \gg \zeta_C$) and for different offsets ρ from the charge trajectory. For a relatively large offset [Fig. 8(a)], the total field, calculated numerically, is in good agreement with its wave component calculated using the stationary point method. Both components have the same order of magnitude, and the beating behavior arises due to the contributions mainly from the two small neighborhoods of ω_p and ω_Σ to the field. For a relatively small offset [Fig. 8(c)], the total field, from numerical calculations, is again in good agreement with its wave component calculated via the small ρ approximation. Both components behave harmonically at a frequency ω_Σ. It should be noted that the E_ρ component is approximately two orders of magnitude larger than E_z, which is explained by a stronger (inversely proportional versus logarithmic) singularity as $\rho \to 0$. The region of the middle offsets [Fig. 8(b)] cannot be described by any of the analytical approximations. However, for $\rho = 50$ μm, the E_z component is still in the beating regime while E_ρ is already in the harmonic regime. The magnitudes of the components are comparable.

B. Field of a finite bunch

It was stressed above that there are singularities in some of the field components on the charge trajectory behind the

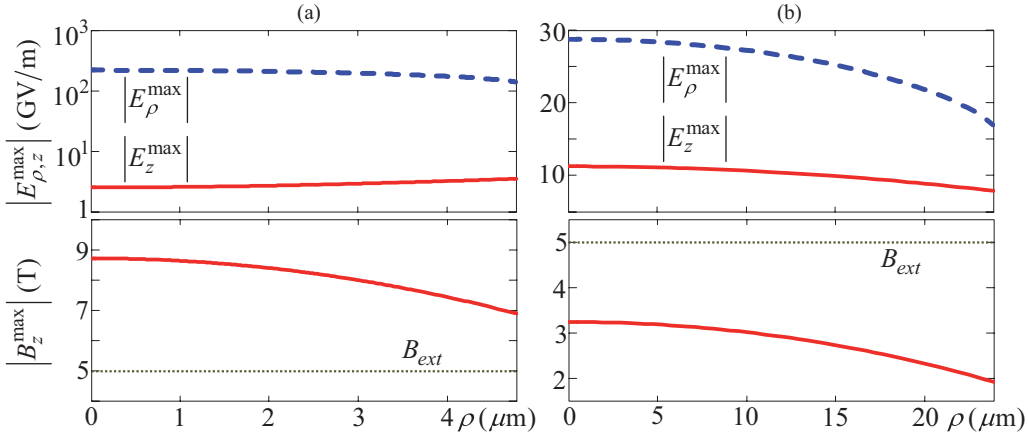

FIG. 10. (Color online) The magnitudes of the longitudinal and orthogonal electric field and longitudinal magnetic field versus ρ, produced by a disk of radius (a) $a = 4.8$ μm and (b) $a = 24$ μm. The other calculation parameters are the same as in Fig. 9.

charge. Therefore, analysis of the small bunch field near the line $\rho = 0$ requires accounting the finite size of the bunch. This problem is particularly relevant in the context of the wakefield acceleration technique, where the wave field of the large driver bunch is used for the acceleration of a relatively small witness bunch [33–35]. One promising version of this method is the plasma wakefield acceleration (PWFA) scheme [36], for which an accelerating field of 40 GeV/m has now been attained [37]. This success has stimulated research activity in this area [38,39].

We can calculate the field of the bunch $\vec{E}^{\rm b}(x,y,\zeta)$, $\vec{H}^{\rm b}(x,y,\zeta)$ using the field of the point charge $\vec{E}(\rho,\zeta)$, $\vec{H}(\rho,\zeta)$ as the Green's function:

$$\{\vec{E}^{\rm b},\vec{H}^{\rm b}\} = \iiint_{V^{\rm b}} dx'dy'd\zeta'\rho^{\rm b}(x',y',\zeta') \times \{\vec{E},\vec{H}\}(\sqrt{(x-x')^2+(y-y')^2},\zeta-\zeta'), \tag{86}$$

where $V^{\rm b}$ is the bunch volume and $\rho^{\rm b}$ is the bunch charge density. The convolution in (86) can be easily calculated for arbitrary $\rho^{\rm b}$ in a region where ζ is sufficiently large ($\zeta < 0$, $|\zeta| \gg \zeta_C$) and ρ is sufficiently small so (A18) is fulfilled; in this case, only the wave component is essential and can be described by the small ρ approximation formulas from (68)–(74) and (A10)–(A17). Indeed, only the strong field components E_ρ^W, E_z^W, and H_z^W are significant in this region. Moreover, the E_ρ^W component is a simple analytical function of ρ and ζ. Although the expressions for the E_z^W and H_z^W components contain complex nonanalytic integral functions of ζ [see the first terms in the formulas (A10) and (A11)], these functions can be replaced by corresponding analytical approximations (by polynomial regression, for example) within the domain of integration in (86). The field of bunches [with the orthogonal dimensions of the bunches satisfying the requirements of the small ρ approach (A18)] can be calculated at large-enough distances behind the bunches without computational difficulties. It should be stressed that this is the region of most interest for PWFA purposes.

For the purposes of illustration, we consider two types of bunches. The first bunch is a uniformly charged, infinitely thin

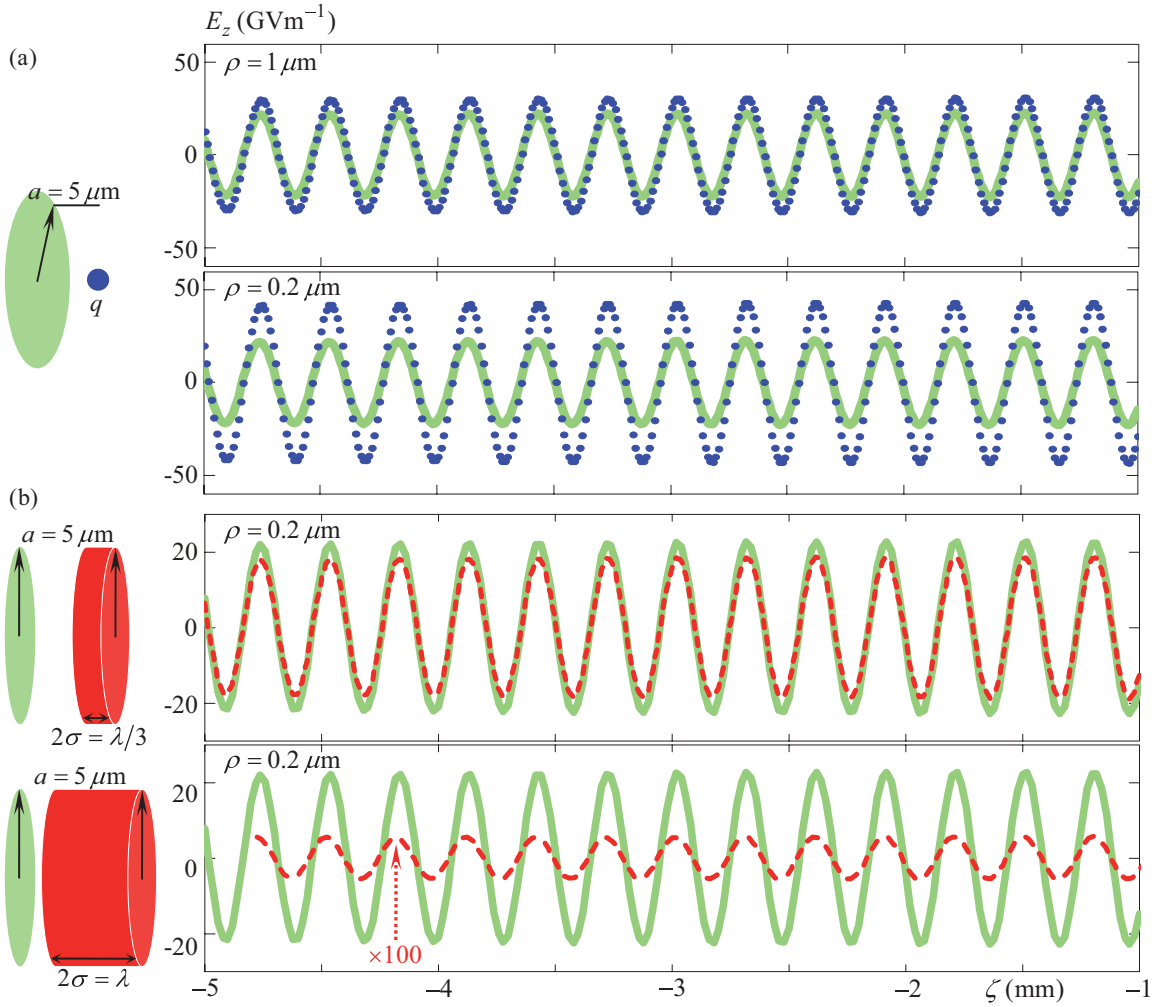

FIG. 11. (Color online) Fields produced by a point charge (dotted blue line), a thin disk (solid green line), and a cylindrical bunch (dashed red line) versus ζ. Calculation parameters are $q = -1$ nC, $\omega_p = 2\pi \times 10^{12}$ s^{-1}, $\omega_h = 0.14\omega_p$ ($B_{\rm ext} = 5$ T), $\beta = 0.999$ ($\gamma = 22$), $\lambda = 2\pi\beta c/\omega_\Sigma = 300\ \mu$m, $\zeta_0 = 3.7$ cm, and ρ_0=12 μm.

disk of radius a with a charge density given by

$$\rho^{\mathrm{d}} = q\Phi(a-\rho)\delta(\zeta)/(\pi a^2). \tag{87}$$

The second bunch is a uniformly charged cylinder with the following charge density:

$$\rho^{\mathrm{c}} = q\Phi(a-\rho)\Phi(\sigma-|\zeta|)/(2\sigma\pi a^2), \tag{88}$$

where a and 2σ are the cylinder radius and length, respectively, and $\Phi(\xi)$ is the Heaviside step function. In these cases, because the integration over x' and y' in (86) uses the point charge field in the domain $\rho\in[0,\,2a]$, the small ρ approach formulas can be applied to calculate (86) for $a<\rho_{\max}/2$ where $\rho_{\max}$ is given by (A18). Moreover, because (87) depends on ζ via the δ function, one can also easily calculate the field produced by a disk with a radius slightly exceeding $\rho_{\max}/2$. In this case, the convolution in (86) utilizes the dependence of the point charge field on the orthogonal coordinate ρ only, and the real complex dependencies $\vec{E}(\rho)$ and $\vec{H}(\rho)$ can be replaced by the corresponding analytical approximations for $\rho > \rho_{\max}$.

Figure 9 compares the behavior of the magnitudes of the main field components versus ρ for a point charge and a charged disk (87). The field produced by the disk is finite at $\rho \to 0$, contrary to the field of the point charge, which is quite naturally. Moreover, the field of the disk varies slowly with ρ.

Figure 10 shows the main components of the field versus ρ, produced by a relatively small disk and a relatively large disk. One can compare the magnitudes of the longitudinal and orthogonal electric field to each other and the magnitude of the longitudinal magnetic field to the magnitude of the external magnetic field. For a relatively small disk radius [Fig. 10(a)], the E_ρ component is approximately two orders of magnitude larger than the E_z component, while these components become comparable for a disk that is 5 times larger [Fig. 10(b)]. The magnitude of the magnetic field produced by a small disk exceeds the external field B_{ext} [Fig. 10(a)], while the larger disk produces a smaller field compared to the external field [Fig. 10(b)].

Figure 11 compares the fields produced by a point charge, a charged disk and a charged cylinder. The disk and cylinder radii a have been chosen such that $a < \rho_{\max}/2$ in the range of varying ζ. Figure 11(a) shows that for a relatively large ρ (comparable to the disk radius), the longitudinal electric field produced by the point charge almost coincides with that produced by the charged disk (this is also can be seen in Fig. 9). With decreasing ρ, the difference becomes essential. Figure 11(b) shows that a short cylinder (on the scale of the wavelength $\lambda = 2\pi\beta c/\omega_\Sigma$) produces a field that almost coincides with that of the disk. The field of the long cylinder is several orders of magnitude smaller than the field of the disk. Obviously, this can be explained by the noncoherency of the fields produced by the different particles inside the large bunch.

These results can be used to further develop the PWFA technique. The electromagnetic field in a cold plasma with a longitudinal external magnetic field has several advantages here. First, we can use the focusing action of the external magnetic field which can be enhanced by the longitudinal magnetic field of the radiated wave. As has been shown, the magnetic field of the wave can exceed the external field for a small enough bunch. Another benefit is that the deflecting orthogonal electric field can be depressed considerably by the external magnetic field.

V. CONCLUSION

In the present work, we have investigated the electromagnetic fields produced by a point charge and a charged bunch moving in a cold magnetized plasma along the external magnetic field. Different equivalent integral representations for the components of the point charge field have been obtained. These representations facilitate both analytical transformations and the development of effective numerical algorithms for computing the fields.

Attention has mainly been focused on the ultrarelativistic motion of a charge. We have divided the field into wave components and quasistatic components. It has been shown that the quasistatic component is only essential at small longitudinal distances from the charge, which is inversely proportional to the Lorentz factor. We have analyzed the wave field in the far-field zone using the stationary point method. One interesting effect is the beating behavior of the field inside the Cherenkov cone, which is explained by the main contributions to the field coming from two small frequency regions. It should be noted that the beating nature of the field is not associated with the existence of ordinary and extraordinary characteristic waves in the medium because only the slow extraordinary wave is excited for the case under consideration.

The wave field in the small neighborhood of the charge trajectory behind the charge has also been analyzed. In this case, we have obtained relatively simple approximate expressions for the field components and have shown that the field exhibits harmonic behavior. The longitudinal electric and magnetic fields show a weak (logarithmic) singularity, while the orthogonal electric field exhibits a stronger (inversely proportional) singularity. The rest of the field components vanish as the distance from the trajectory tends to zero. These properties are similar to those of the "plasma trace," which is usually encountered in isotropic media. An important difference between the two cases consists of the presence of a large wave magnetic field in the vicinity of the trajectory. On the other hand, the longitudinal electric field does not depend on the external magnetic field and coincides with that of the "plasma trace." In contrast, the magnitude of the orthogonal electric field decreases while the magnitude of the longitudinal magnetic field increases with an increasing external magnetic field.

By suitably transforming the integration path in the complex plane, we have developed an efficient numerical algorithm for the computation of the point charge field at arbitrary distances. The field patterns obtained using this method were in good agreement with those obtained by using the analytical approximations in the domain of their validity. The field behavior in the "middle" zone, which cannot be calculated using the approximate techniques, has been analyzed. In particular, it has been shown that the longitudinal electric field can be in the beating regime (similar to the far-field zone) while the orthogonal electric field is already in the harmonic regime (similar to the neighborhood of the trajectory).

The expressions for the wave field in the vicinity of the charge motion line have been effectively utilized to calculate the fields produced by two types of bunches. The fields produced by a point charge, a disk, and a cylinder have been compared to each other. The fields of the point charge and the thin disk almost coincide at distances on the order of the disk radius from the charge motion line. The orthogonal electric field can be several orders of magnitude larger than the longitudinal electric field for a relatively small disk, while the difference between the orthogonal and longitudinal components decreases with increasing disk radius. The longitudinal magnetic field can exceed the external magnetic field for a small enough disk. A short cylindrical bunch with a length of one third of the wavelength produces a field that almost coincides with the field of an infinitely thin disk. In contrast, the field for a bunch that is one wavelength long is much smaller than the field of the disk. This effect highlights the incoherent summation of fields produced by charges of a long bunch.

These results can be implemented in all areas where charged particles in cold plasma are encountered. The approaches developed here facilitate quick and efficient numerical calculation of wakefields produced by small bunches of arbitrary configuration. This approach is based on computing the convolution integral with analytical functions and requires neither expensive numerical simulation suites nor a large amount of computer resources.

ACKNOWLEDGMENTS

This research was supported by St. Petersburg State University, the Dmitry Zimin "Dynasty" Foundation, and the Russian Foundation for Basic Research (Grant No. 12-02-31258).

APPENDIX A: WAVE-FIELD EXPANSION AT SMALL VALUES OF ρ

Here, we present the results for treating the wave integrals (56) and (57) in the vicinity of the charge trajectory. First, let us specify a region δ such that the function $s_e(\omega)$ can be substituted by the expression (66) for $\omega_\Sigma - \delta < \omega < \omega_\Sigma$, with a given accuracy. For example, δ can be defined as follows:

$$\left|\left(s_e^2(\omega_\Sigma - \delta) - \sigma_e^2/\delta\right)s_e^{-2}(\omega_\Sigma - \delta)\right| = 10^{-m}, \qquad \text{(A1)}$$

where the fixed integer $m > 0$ determines the accuracy. The integrals (56) and (57) can be rewritten as follows:

$$\begin{Bmatrix} E^W_{\rho,\varphi,z} \\ H^W_{\rho,\varphi,z} \end{Bmatrix} = \begin{Bmatrix} \tilde{E}^W_{\rho,\varphi,z} + \tilde{\tilde{E}}^W_{\rho,\varphi,z} \\ \tilde{H}^W_{\rho,\varphi,z} + \tilde{\tilde{H}}^W_{\rho,\varphi,z} \end{Bmatrix}. \qquad \text{(A2)}$$

Here, the primary summands (shown with a single tilde) are integrals of the form $\int_{\omega_p}^{\omega_\Sigma-\delta} d\omega$. The secondary summands (shown with a double tilde) are integrals of the form $\int_{\omega_\Sigma-\delta}^{\omega_\Sigma} d\omega$. The integrands of these expressions are the same as in formulas (56) and (57). Because the function $s_e(\omega)$ is limited in the interval $\omega_p < \omega < \omega_\Sigma - \delta$, the Bessel functions in the single tilde summands can be expanded into a series [31],

$$\begin{aligned} J_0(\rho s_e) &\underset{\rho\to 0}{\approx} 1 - (\rho s_e)^2/4, \\ J_1(\rho s_e) &\underset{\rho\to 0}{\approx} \rho s_e/2 - (\rho s_e)^3/16, \end{aligned} \qquad \text{(A3)}$$

in the issue, single tilde summands behave as polynomials of the second or third degree with respect to ρ as $\rho \to 0$.

The integrands in the double tilde summands in (A2) can be simplified further. The nondivergent summands can be neglected compared to the divergent summands ($s_e^2, \varepsilon_1 s_e^2 \sim s_e$) so the slowly varying functions can then be factored out of the integral. In the issue we have

$$\begin{aligned} \tilde{\tilde{E}}^W_\rho &\sim \int_{\omega_\Sigma-\delta}^{\omega_\Sigma} s_e^3 J_1(\rho s_e) d\omega \\ &= \int_{\omega_\Sigma-\delta}^{\omega_\Sigma} \frac{\sigma_e^3}{(\omega_\Sigma - \omega)^{3/2}} J_1\left(\frac{\rho\sigma_e}{\sqrt{\omega_\Sigma - \omega}}\right) d\omega, \end{aligned} \qquad \text{(A4)}$$

$$\begin{aligned} \left\{\tilde{\tilde{E}}^W_z, \tilde{\tilde{H}}^W_z\right\} &\sim \int_{\omega_\Sigma-\delta}^{\omega_\Sigma} s_e^2 J_0(\rho s_e) d\omega \\ &= \int_{\omega_\Sigma-\delta}^{\omega_\Sigma} \frac{\sigma_e^2}{\omega_\Sigma - \omega} J_0\left(\frac{\rho\sigma_e}{\sqrt{\omega_\Sigma - \omega}}\right) d\omega, \end{aligned} \qquad \text{(A5)}$$

$$\begin{aligned} \left\{\tilde{\tilde{E}}^W_\varphi, \tilde{\tilde{H}}^W_{\rho,\varphi}\right\} &\sim \int_{\omega_\Sigma-\delta}^{\omega_\Sigma} s_e J_1(\rho s_e) d\omega \\ &= \int_{\omega_\Sigma-\delta}^{\omega_\Sigma} \frac{\sigma_e}{\sqrt{\omega_\Sigma - \omega}} J_1\left(\frac{\rho\sigma_e}{\sqrt{\omega_\Sigma - \omega}}\right) d\omega. \end{aligned} \qquad \text{(A6)}$$

Introducing a new variable $\xi = \rho\sigma_e/\sqrt{\omega_\Sigma - \omega}$ in (A4)–(A6), one obtains

$$\tilde{\tilde{E}}^W_\rho \sim \frac{1}{\rho}\int_{\rho\sigma_e/\sqrt{\delta}}^{\infty} J_1(\xi) d\xi, \qquad \text{(A7)}$$

$$\begin{aligned} \left\{\tilde{\tilde{E}}^W_z, \tilde{\tilde{H}}^W_z\right\} &\sim \int_{\rho\sigma_e/\sqrt{\delta}}^{\infty} J_0(\xi)\xi^{-1} d\xi, \\ \left\{\tilde{\tilde{E}}^W_\varphi, \tilde{\tilde{H}}^W_{\rho,\varphi}\right\} &\sim \rho\int_{\rho\sigma_e/\sqrt{\delta}}^{\infty} J_1(\xi)\xi^{-2} d\xi. \end{aligned} \qquad \text{(A8)}$$

Expressions (A7) and (A8) show that for finite $\rho \neq 0$, the integrals (56) and (57) are convergent. However, expression (A7) diverges as $\rho \to 0$, and the integrals in (A8) also contain divergent terms. Indeed, one can put $\rho = 0$ in the lower limit of the integral (A7), therefore, $E^W_\rho \sim \text{const}/\rho$ as $\rho \to 0$. The integrals in (A8) can be approximated by the following scheme. Let us suppose that ρ is sufficiently small so

$$\rho < \rho_0 \equiv \sqrt{\delta}/\sigma_e. \qquad \text{(A9)}$$

When (A9) is fulfilled, $\rho\sigma_e/\sqrt{\delta} < 1$ and $\xi = 1$ lies within the integration interval. Each of integrals in (A8) then can be divided into two, such that the integration is performed from $\rho\sigma_e/\sqrt{\delta}$ to 1 in the first integral and from 1 to ∞ in the second integral. The tail integrals from 1 to ∞ are convergent and do not depend on ρ. The integrals from $\rho\sigma_e/\sqrt{\delta}$ to 1 can be approximated by expanding the Bessel functions $J_0(\xi)$ and $J_1(\xi)$ into a series similar to (A3). The first terms in the Bessel function expansions give logarithmic terms, while the second terms produce quadratic polynomials in ρ for the integrals in (A8). As a result, we obtain the decomposition (68) and (69), where the dominant contributions are given by formulas (70)–(74),

and the corrections are expressed as follows:

$$E_z^{W0} = \frac{q\beta}{\omega_p^2\omega_h}\int_{\omega_p}^{\omega_\Sigma-\delta}\frac{\omega\left(\omega^2-\omega_h^2\right)}{\sqrt{\omega^2-\omega_c^2}}\left[\frac{\omega^2}{c^2}\left(\varepsilon_2^2-\varepsilon_1^2+\frac{2\varepsilon_1}{\beta^2}-\frac{1}{\beta^4}\right)+s_e^2\left(\varepsilon_1-\frac{1}{\beta^2}\right)\right]\cos\left(\frac{\omega\zeta}{\upsilon}\right)d\omega$$
$$+\frac{q\beta\omega_\Sigma}{\omega_h\sqrt{\omega_\Sigma^2-\omega_c^2}}\left\{\frac{\upsilon}{\zeta}\left[\frac{\omega_\Sigma^2}{c^2}\varepsilon_2^2(\omega_\Sigma)-\frac{2\omega_\Sigma\sigma_e^2}{\omega_p^2}-\frac{\omega_\Sigma^2}{\upsilon^2\beta^2}\right]\left[\sin\left(\frac{\omega_\Sigma\zeta}{\upsilon}\right)-\sin\left(\frac{(\omega_\Sigma-\delta)\zeta}{\upsilon}\right)\right]\right.$$
$$\left.-\frac{2\sigma_e^2}{\beta^2}\left[\cos\left(\frac{\omega_\Sigma\zeta}{\upsilon}\right)M_1+\sin\left(\frac{\omega_\Sigma\zeta}{\upsilon}\right)M_2\right]\right\}, \tag{A10}$$

$$H_z^{W0} = -q\int_{\omega_p}^{\omega_\Sigma-\delta}\frac{s_e^2}{\sqrt{\omega^2-\omega_c^2}}\sin\left(\frac{\omega\zeta}{\upsilon}\right)d\omega-\frac{2q\sigma_e^2}{\sqrt{\omega_\Sigma^2-\omega_c^2}}\left[\sin\left(\frac{\omega_\Sigma\zeta}{\upsilon}\right)M_1-\cos\left(\frac{\omega_\Sigma\zeta}{\upsilon}\right)M_2\right], \tag{A11}$$

$$E_\varphi^{W0} = -\beta H_\rho^{W0} = \frac{-q}{2\omega_p}\int_{\omega_p}^{\omega_\Sigma-\delta}\frac{\omega s_e^2}{\sqrt{\omega^2-\omega_c^2}}\cos\left(\frac{\omega\zeta}{\upsilon}\right)d\omega-\frac{q\omega_\Sigma\sigma_e^2}{c\sqrt{\omega_\Sigma^2-\omega_c^2}}\left[\cos\left(\frac{\omega_\Sigma\zeta}{\upsilon}\right)M_3+\sin\left(\frac{\omega_\Sigma\zeta}{\upsilon}\right)M_2\right], \tag{A12}$$

$$H_\varphi^{W0} = \frac{qc^2\beta}{2\omega_p^3\omega_h}\int_{\omega_p}^{\omega_\Sigma-\delta}\frac{s_e^2\left(\omega^2-\omega_h^2\right)}{\sqrt{\omega^2-\omega_c^2}}\left[\frac{\omega^2}{c^2}\left(\varepsilon_2^2-\varepsilon_1^2+\frac{\varepsilon_1}{\beta^2}\right)+\varepsilon_1 s_e^2\right]\sin\left(\frac{\omega\zeta}{\upsilon}\right)d\omega$$
$$+\frac{qc^2\beta\sigma_e^2}{\omega_p\omega_h\sqrt{\omega_\Sigma^2-\omega_c^2}}\left[\frac{\omega_\Sigma^2}{c^2}\varepsilon_2^2(\omega_\Sigma)-\frac{2\omega_\Sigma\sigma_e^2}{\omega_p^2}\right]\left[\sin\left(\frac{\omega_\Sigma\zeta}{\upsilon}\right)M_3-\cos\left(\frac{\omega_\Sigma\zeta}{\upsilon}\right)M_2\right], \tag{A13}$$

$$M_1 = \begin{cases}\int_1^\infty\frac{J_0(\xi)}{\xi}d\xi+\ln\left(\frac{\omega_p\sqrt{\upsilon}}{c\sigma_e\sqrt{|\zeta|}}\right)+A_c-\frac{1}{4} & \text{for}\quad |\zeta|>\zeta_0,\quad \rho<\rho_0\sqrt{\zeta_0/|\zeta|},\\ \int_1^\infty\frac{J_0(\xi)}{\xi}d\xi+\ln\left(\frac{\omega_p\sqrt{\delta}}{c\sigma_e}\right)-\frac{1}{8}\frac{\zeta^2}{\upsilon^2}\delta^2-\frac{1}{8} & \text{for}\quad |\zeta|<\zeta_0,\quad \rho<\rho_0,\end{cases} \tag{A14}$$

$$M_2 = \begin{cases}A_s-\frac{1}{2} & \text{for}\quad |\zeta|>\zeta_0,\quad \rho<\rho_0\sqrt{\zeta_0/|\zeta|},\\ -\frac{1}{2}\frac{|\zeta|}{\upsilon}\delta & \text{for}\quad |\zeta|<\zeta_0,\quad \rho<\rho_0,\end{cases} \tag{A15}$$

$$M_3 = \begin{cases}2\int_1^\infty\frac{J_1(\xi)}{\xi^2}d\xi+\ln\left(\frac{\omega_p\sqrt{\upsilon}}{c\sigma_e\sqrt{|\zeta|}}\right)+A_c-\frac{3}{16} & \text{for}\quad |\zeta|>\zeta_0,\quad \rho<\rho_0\sqrt{\zeta_0/|\zeta|},\\ 2\int_1^\infty\frac{J_1(\xi)}{\xi^2}d\xi+\ln\left(\frac{\omega_p\sqrt{\delta}}{c\sigma_e}\right)-\frac{1}{8}\frac{\zeta^2}{\upsilon^2}\delta^2-\frac{1}{16} & \text{for}\quad |\zeta|<\zeta_0,\quad \rho<\rho_0,\end{cases} \tag{A16}$$

$$A_c = \int_{\sqrt{\upsilon/|\zeta|}}^{\sqrt{\delta}}\cos(\zeta\xi^2/\upsilon)\xi^{-1}\,d\xi,\quad A_s = \int_{\sqrt{\upsilon/|\zeta|}}^{\sqrt{\delta}}\sin(\zeta\xi^2/\upsilon)\xi^{-1}\,d\xi, \tag{A17}$$

where $\zeta_0 \equiv \upsilon/\delta$ and δ is defined by (A1). The region of validity for the approximation can be written in the following form:

$$\rho<\rho_{\max}\equiv\begin{cases}\rho_0 & \text{for}\quad |\zeta|<\zeta_0,\\ \rho_0\sqrt{\zeta_0/|\zeta|} & \text{for}\quad |\zeta|>\zeta_0,\end{cases} \tag{A18}$$

and is shown as the dashed region in Fig. 12. Note that because a logarithm is a weak singularity, the constant terms can have significant contributions, for example, for large values of $|\zeta|$.

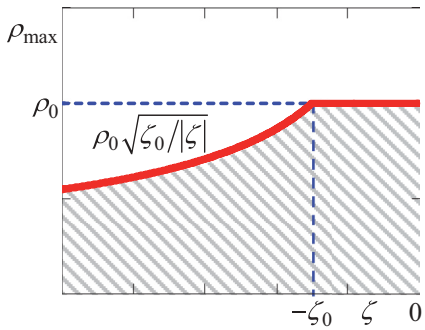

FIG. 12. (Color online) The region of validity (shown with dashes) in the (ρ, ζ) plane for the approximations given by (68)–(74) and (A10)–(A17) for the wave components of the field.

In concluding this section, one should say a few words about the numerical calculation of the wave components via exact formulas (56) and (57). As mentioned above, the function $s_e(\omega)$ is limited in the interval $\omega_p < \omega < \omega_\Sigma - \delta$ so there are no difficulties in calculating the single tilde summands. However, the "tail" integrals (A8) for E_φ^W and $H_{\rho,\varphi}^W$ exhibit the steepest convergence at $\xi\to\infty$ [$\sim\cos(\xi - 3\pi/4)/\xi^{5/2}$], while those for E_z^W and H_z^W exhibit a slower convergence [$\sim\cos(\xi-\pi/4)/\xi^{3/2}$], and the integral (A7) for E_ρ^W exhibits the slowest convergence [$\sim\cos(\xi-3\pi/4)\xi^{1/2}$]. The numerical calculation of the "tails" (A7) and (A8) requires the integration interval to be restricted by a value $\xi_{\max}$ so integrals from $\xi_{\max}$ to ∞ can be neglected. Thus, $\xi_{\max}$ for the calculation of E_ρ^W should take the largest value, while $\xi_{\max}$ for calculating E_z^W and H_z^W should take smaller values and $\xi_{\max}$ for calculating E_φ^W and $H_{\rho,\varphi}^W$ should take the smallest value. Moreover, because the integration step size $\delta\xi$ should be at least several times smaller than the oscillation period (which equals approximately unity), increasing $\xi_{\max}$ essentially leads to increasing the calculation time.

APPENDIX B: INVESTIGATION OF THE STATIONARY-POINTS EQUATIONS (80)

Here, we investigate possibilities of solving the equations (80) to determine the stationary points $\omega_{s1,2}$. The properties of $ds_e/d\omega$ are examined in the interval $[\omega_p, \omega_\Sigma]$ or, equivalently, in the interval $[u_1, u_2]$ [recall that u_1 corresponds to ω_p, while u_2 corresponds to ω_Σ, see (51)]. Using (47), one can rewrite the derivative of s_e with respect to ω as follows:

$$\frac{ds_e}{d\omega} = \frac{ds_e}{du}\frac{du}{d\omega} = \frac{1}{2s_e}\frac{ds_e^2}{du}\frac{du}{d\omega}, \tag{B1}$$

where $du/d\omega = \omega/u$. Because $s_e > 0$ and $du/d\omega > 0$ within $[\omega_p, \omega_\Sigma]$, $ds_e/d\omega$ has the same sign as ds_e^2/du. The derivative ds_e^2/du is expressed as follows:

$$\begin{aligned} \frac{ds_e^2}{du} &= \frac{P_B(u)}{c^2(u-u_2)^2}, \\ P_B(u) &= B_3u^3 + B_2u^2 + B_1u + B_0, \end{aligned} \tag{B2}$$

where for the ultrarelativistic case $\gamma \gg 1$, we have

$$\begin{aligned} B_3 &\approx \frac{-2}{\gamma^2-1}, \quad B_2 \approx \frac{2\omega_h(2\gamma^2-1)}{\gamma(\gamma^2-1)^{3/2}}, \\ B_1 &\approx \frac{-\omega_h^2(2\gamma^2-1)^2}{2\gamma^2(\gamma^2-1)^2}, \quad B_0 \approx \frac{\omega_p^2\omega_h\gamma}{\sqrt{\gamma^2-1}}. \end{aligned} \tag{B3}$$

Using (B3), one can show that $P_B(u_1) \approx P_B(u_2) \approx \omega_p^2\omega_h[1 + 1/(2\gamma^2)] > 0$ for $\gamma \gg 1$. The extrema of $P_B(u)$ are determined by the following equation:

$$P_B'(u) = 3B_3u^2 + 2B_2u + B_1 = 0, \tag{B4}$$

where $P_B'(u) = dP_B/du$. The roots of (B4) are $u_2/3$ and u_2. Because $P_B''(u_2/3) \approx 4\omega_h/\gamma^2 > 0$ for $\gamma \gg 1$, $P_B(u)$ possesses a minimum at $u = u_2/3$. Because $P_B(u_2/3) \approx \omega_p^2\omega_h > 0$ for $\gamma \gg 1$, then $P_B(u) > 0$ and $ds_e^2/du > 0$ over the whole interval $[u_1, u_2]$ and, therefore, $ds_e/d\omega > 0$ over $[\omega_p, \omega_\Sigma]$. Thus, we have proved that the derivative of s_e with respect to ω is positive within the range of radiated frequencies for the ultrarelativistic case. This means that equation (80) with the plus sign has no solutions.

To obtain the extrema of the function $ds_e/d\omega$, the second derivative of s_e is equated to zero:

$$\begin{aligned} \frac{d^2s_e}{d\omega^2} &= \frac{1}{2s_e}\left\{\frac{ds_e^2}{du}\frac{d^2u}{d\omega^2} + \left[\frac{d^2s_e^2}{du^2} - \frac{1}{2s_e^2}\left(\frac{ds_e^2}{du}\right)^2\right]\left(\frac{du}{d\omega}\right)^2\right\} \\ &= 0. \end{aligned} \tag{B5}$$

For $\gamma \gg 1$, the expression in the figure brackets of (B5) can be presented in the following form:

$$-\frac{4\omega_p^4\omega_h\left[u^3 - \frac{\omega_h}{4}u^2 + \frac{3\omega_p^2}{2}u - \frac{3\omega_p^2\omega_h}{4}\right] - \frac{\Lambda(u)}{\gamma^2}}{2c^2\omega_p^2u^3(u-\omega_h)^3} = 0, \tag{B6}$$

where

$$\begin{aligned} \Lambda(u) &= 4\omega_p^4(u-\omega_h)\left(u^3 - 2\omega_hu^2 + \omega_hu - \frac{\omega_p^2\omega_h}{4}\right) \\ &\quad - 2\omega_p^4\left(u^2+\omega_p^2\right)\left[2\frac{u^4}{\omega_p^2} - 2\frac{\omega_hu^3}{\omega_p^2} - \omega_hu - \omega_h^2\right. \\ &\quad \left. + \left(4\omega_p^4\omega_hu - \omega_p^4\omega_h^2\right)\left(\frac{\omega_h}{2u} - \frac{u^2-\omega_hu}{\omega_p^2}\right)\right]. \end{aligned} \tag{B7}$$

If we neglect the term $\sim\gamma^{-2}$ in (B6), we obtain the following equation for the extrema of $ds_e/d\omega$:

$$u^3 + \frac{u^2\omega_h}{4} + \frac{3u\omega_p^2}{2} - \frac{3\omega_p^2\omega_h}{4} = 0. \tag{B8}$$

The derivative of (B8) results in the following equation:

$$3u^2 + u\omega_h/2 + 3\omega_p^2/2 = 0, \tag{B9}$$

the determinant of which is

$$D = \left(\omega_h^2 - 72\omega_p^2\right)/4. \tag{B10}$$

For $D < 0$, (B9) does not have real solutions and the polynomial on the left-hand side of (B8) has no extrema. Therefore, (B8) has a single real solution and $ds_e/d\omega$ has a single extremum when the following inequality is fulfilled:

$$\omega_h < 6\sqrt{2}\omega_p \approx 8.5\omega_p. \tag{B11}$$

Condition (B11) can be understood as a requirement that the external magnetic field $H_{\text{ext}} \sim \omega_h$ not be very large. If (B11) is satisfied, the single real root of (B8) $u^{(0)}$ can be found exactly:

$$u^{(0)} = \frac{(a_0+36b_0)^{\frac{2}{3}} - 72\omega_p^2 + \omega_h^2 + \omega_h(a_0+36b_0)^{\frac{1}{3}}}{12(a_0+36b_0)^{1/3}}, \tag{B12}$$

where

$$\begin{aligned} a_0 &= 540\omega_p^2\omega_h + \omega_h^3, \\ b_0 &= \omega_p\sqrt{288\omega_p^4 + 213\omega_p^2\omega_h^2 + \omega_h^4}. \end{aligned} \tag{B13}$$

For $\omega_h \ll \omega_p$, expression (B12) simplifies to

$$u^{(0)} \underset{\gamma\gg1,\ \omega_p\gg\omega_h}{\approx} \omega_h/2. \tag{B14}$$

Equation (B6) can be solved when the term $\sim\gamma^{-2}$ is taken into account by using the successive approximation method. Using the ansatz $u = u^{(0)} + u^{(1)}/\gamma^2$ and substituting it into (B6), one finds

$$u^{(1)} = \frac{\Lambda(u^{(0)})}{4\omega_p^4\omega_h\left[3(u^{(0)})^2 - u^{(0)}\omega_h/2 + 3\omega_p^2/2\right]}. \tag{B15}$$

From (48), (B1), and (B2), $ds_e/d\omega \to +\infty$ as both $\omega \to \omega_p$ (or $u \to u_1$) and $\omega \to \omega_\Sigma$ (or $u \to u_2$); therefore, the extremum that has been found is a minimum. When the external magnetic field is not very strong in the sense of (B11), the function $ds_e/d\omega$ has a single minimum at the frequency ω_{s0}, which can be calculated via the formula

$$\omega_{s0} = \sqrt{\omega_c^2 + (u^{(0)} + u^{(1)}/\gamma^2)^2}, \tag{B16}$$

where ω_c is given by (37) and (39). In the special case of $\gamma \gg 1$ and $\omega_h \ll \omega_p$, one obtains the following

expressions:

$$\omega_{s0} \approx \omega_p\left(1+\frac{\omega_h^2}{8\omega_p^2}\right), \quad s'_{e\,\min} \equiv \frac{ds_e(\omega_{s0})}{d\omega} \approx \frac{4\omega_p^2}{\omega_h^2}. \tag{B17}$$

The characteristic dependence of $ds_e/d\omega$ on ω is presented in Fig. 5(a).

Next, approximate expressions for the stationary points $\omega_{s1,2}$ are found. Strictly speaking, equation (B5) reduces to (B8) only for $\gamma \to \infty$ or $\beta \to 1$. For $\beta = 1$, (B1) can be presented in the following form:

$$\frac{ds_e}{d\omega} = \frac{\omega_p\omega_h}{2c}\frac{\omega}{\left(\omega^2-\omega_p^2\right)^{3/4}\left(\omega_h-\sqrt{\omega^2-\omega_p^2}\right)^{3/2}}. \tag{B18}$$

For $|\zeta| \gg \zeta_{\min} \equiv \rho\upsilon s'_{e\,\min}$ one obtains $\omega_{s1} \to \omega_p$ and $\omega_{s2} \to \omega_\Sigma$, so two separate approximate equations can be written for the stationary points:

$$\begin{aligned} \omega_{s1}\colon \quad & \frac{|\zeta|}{\rho\upsilon} \approx \frac{\omega_p^2\omega_h/(2c)}{\left(\omega^2-\omega_p^2\right)^{3/4}\omega_h^{3/2}}, \\ \omega_{s2}\colon \quad & \frac{|\zeta|}{\rho\upsilon} \approx \frac{\omega_\Sigma\omega_p\omega_h/(2c)}{\omega_h^{3/2}\left(\omega_h-\sqrt{\omega^2-\omega_p^2}\right)^{3/2}}. \end{aligned} \tag{B19}$$

The solution of (B19) results in the formulas given by (83). For the general case, stationary points can be found numerically using the approximate expressions in (83) as initial guesses.

[1] P. A. Čerenkov, Phys. Rev. **52**, 378 (1937).
[2] I. E. Tamm, J. Phys. USSR **1**, 439 (1939).
[3] E. Fermi, Phys. Rev. **57**, 485 (1940).
[4] B. M. Bolotovskii, Usp. Fiz. Nauk **62**, 201 (1957).
[5] J. V. Jelley, *Čerenkov Radiation and Its Applications* (Pergamon, London, 1958).
[6] V. P. Zrelov, *Vavilov-Cherenkov Radiation in High-Energy Physics* (Israel Program for Scientific Translations, Jerusalem, 1970).
[7] I. M. Frank, *Vavilov-Cherenkov Radiation: Theoretical Aspects* (Nauka, Moscow, 1988) in Russian.
[8] V. L. Ginzburg, J. Phys. USSR **3**, 101 (1940).
[9] V. L. Ginzburg and V. N. Tsytovich, *Transition Radiation and Transition Scattering* (Hilger, London, 1990).
[10] J. Lu, T. M. Grzegorczyk, Y. Zhang, J. Pacheco Jr., B.-I. Wu, J. A. Kong, and M. Chen, Opt. Express **11**, 723 (2003).
[11] Z. Y. Duan, B. I. Wu, S. Xi, H. S. Chen, and M. Chen, Prog. Electromagn. Res. **90**, 75 (2009).
[12] S. Antipov, L. Spentzouris, W. Liu, W. Gai, and J. G. Power, J. Appl. Phys. **102**, 034906 (2007).
[13] S. N. Galyamin, A. V. Tyukhtin, A. Kanareykin, and P. Schoessow, Phys. Rev. Lett. **103**, 194802 (2009).
[14] S. N. Galyamin and A. V. Tyukhtin, Phys. Rev. B **81**, 235134 (2010).
[15] E. S. Belonogaya, S. N. Galyamin, and A. V. Tyukhtin, J. Opt. Soc. Am. B **28**, 2871 (2011).
[16] S. N. Galyamin and A. V. Tyukhtin, Phys. Rev. E **84**, 056608 (2011).
[17] V. V. Vorobev and A. V. Tyukhtin, Phys. Rev. Lett. **108**, 184801 (2012).
[18] D. E. Fernandes, S. I. Maslovski, and M. G. Silveirinha, Phys. Rev. B **85**, 155107 (2012).
[19] V. L. Ginzburg, *The Propagation of Electromagnetic Waves in Plasma* (Pergamon, London, 1964).
[20] A. A. Kolomenskii, Compt. Rend. Acad. Sci. USSR **106**, 982 (1956).
[21] A. G. Sitenko and A. A. Kolomenskii, Sov. Phys. JETP **30**, 511 (1956).
[22] I. A. Akhiezer, Sov. Phys. JETP **13**, 667 (1961).
[23] A. B. Kitsenko, Compt. Rend. Acad. Sci. USSR **145**, 305 (1962).
[24] M. Kuzelev, Plasma Phys. Rep. **34**, 284 (2008).
[25] V. A. Balakirev, V. I. Miroshnichenko, V. E. Storizhko, and A. P. Tolstoluzhsky, Probl. At. Sci. Technol. **2**, 181 (2010).
[26] D. De Zutter and D. De Vleeschauwer, J. Appl. Phys. **59**, 4146 (1986).
[27] G. N. Afanasiev and V. G. Kartavenko, J. Phys. D: Appl. Phys. **31**, 2760 (1998).
[28] G. N. Afanasiev, *Vavilov-Cherenkov and Synchrotron Radiation: Founadations and Applications* (Springer, Berlin, 2004).
[29] A. V. Tyukhtin and S. N. Galyamin, Phys. Rev. E **77**, 066606 (2008).
[30] L. D. Landau and E. M. Lifshitz, *Electrodynamics of Continuous Media* (Pergamon, London, 1984).
[31] H. Bateman and A. Erdelyi, *Higher Transcendental Functions* (McGraw-Hill, New York, 1953).
[32] L. B. Felsen and N. Marcuvitz, *Radiation and Scattering of Waves* (Wiley Interscience, New York, 2003).
[33] W. Gai, P. Schoessow, B. Cole, R. Konecny, J. Norem, J. Rosenzweig, and J. Simpson, Phys. Rev. Lett. **61**, 2756 (1988).
[34] S. Antipov, C. Jing, M. Fedurin, W. Gai, A. Kanareykin, K. Kusche, P. Schoessow, V. Yakimenko, and A. Zholents, Phys. Rev. Lett. **108**, 144801 (2012).
[35] B. Jiang, C. Jing, P. Schoessow, J. Power, and W. Gai, Phys. Rev. ST Accel. Beams **15**, 011301 (2012).
[36] C. Joshi and T. Katsouleas, Phys. Today **56**, 47 (2003).
[37] I. Blumenfeld, C. E. Clayton, F.-J. Decker, M. J. Hogan, C. Huang, R. Ischebeck, R. Iverson, C. Joshi, T. Katsouleas, N. Kirby, W. Lu, K. A. Marsh, W. B. Mori, P. Muggli, E. Oz, R. H. Siemann, D. Walz, and M. Zhou, Nature **445**, 741 (2007).
[38] A. Caldwell, K. Lotov, A. Pukhov, and F. Simon, Nat. Phys. **5**, 363 (2009).
[39] C. Joshi and V. Malka, New J. Phys. **12**, 045003 (2010).